

SymAR: Symmetry Abstractions and Refinement for Accelerating Scenarios with Neural Network Controllers Verification

Hussein Sibai, Yangge Li, and Sayan Mitra
University of Illinois at Urbana-Champaign
Coordinated Science Laboratory
{sibai2,li213,mitras}@illinois.edu

ABSTRACT

We present a Symmetry-based abstraction refinement algorithm SymAR that is directed towards safety verification of large-scale scenarios with complex dynamical systems. The abstraction maps modes with symmetric dynamics to a single abstract mode and refinements recursively split the modes when safety checks fail. We show how symmetry abstractions can be applied effectively to closed-loop control systems, including non-symmetric deep neural network (DNN) controllers. For such controllers, we transform their inputs and outputs to enforce symmetry and make the closed loop system amenable for abstraction. We implemented SymAR in Python and used it to verify paths with 100s of segments in 2D and 3D scenarios followed by a six dimensional DNN-controlled quadrotor, and also a ground vehicle. Our experiments show significant savings, up to 10x in some cases, in verification time over existing methods.

1 INTRODUCTION

The set of states that can be reached by a hybrid or dynamical system over a given time horizon is called the reachable set. Computing or approximating the reachable set, known as *reachability analysis*, is a fundamental subroutine for formal verification, controller synthesis, and monitoring. Notwithstanding the undecidability results [13], and the curse of dimensionality plaguing the early algorithms, over the last decade, the hybrid systems community has pushed the reach of reachability analysis tools from small, academic, linear models to realistic nonlinear models [1, 4, 6, 11, 18], linear models with millions of dimensions [3, 12], and deep neural networks (DNN) and DNN-controlled systems [8, 14, 21]. This remarkable progress has been accomplished by and large by focusing on one half of the hybrid reachability problem—namely the the continuous part.

Specifically, (a) exploiting ideas from control theory and real analysis for approximating solutions of dynamical systems [4, 11], and (b) invention of clever new data structures like zonotopes [1], support functions [1, 12] and generalized star sets [3], for representing and manipulating sets of solutions of dynamical systems. The problem studied in this paper addresses challenges arising from reachability analysis of models with complex continuous *and* discrete dynamics.

Consider the scenario verification problem illustrated in Figure 1a: An autonomous or semi-autonomous vehicle system driving in a complex environment. There are many obstacles in the map. The vehicle has nonlinear-dynamics. It may be using a complicated controller function for tracking waypoints, for example, DNNs. A high-level *planner* (MP) generates a set of possible paths or waypoint sequences using a motion planning algorithm like *Rapidly Expanding Random Trees* (RRT) [16] that *does not* consider the dynamics

of the vehicle nor the state estimation errors. Then, the verification task for this system is to check which parts of this plan can be safely executed by the vehicle, without running into the obstacles. Such a problem arises in online planning where many options or paths have to be evaluated quickly. Naively viewing this system as a hybrid automaton evolving in the vehicle’s state space with the modes defined by the segments of the planner, will lead to a hybrid model with hundreds or even thousands of modes and transitions. Indeed, many of these modes will be geometric transformations of each other, but current hybrid reachability tools cannot take advantage of this structure. Analyzing automaton models with large number of modes and transitions is challenging as (a) the error in over-approximations grows with the number of transitions, and (b) the size of the data structures that have to be maintained to track reachable sets grow combinatorially with the length of the mode sequences, and (c) the time needed to compute the reachable set grows with the number of transitions and the over-approximation error. An example of this is shown in Figure 1b.

In this paper, we show how symmetry abstractions can be used to tackle scenario verification problems with existing reachability analysis tools. The notion of symmetry abstractions was introduced in [20]. There, it was shown that these abstractions significantly reduce the number of modes and edges of a given automaton \mathcal{A} . These abstractions achieve this reduction by grouping all modes of \mathcal{A} that share symmetric continuous dynamics in a single representative mode of the abstract automaton \mathcal{A}_v . It was further shown how the reachable set $Reach_{\mathcal{A}_v}$ of \mathcal{A}_v can be transformed using symmetry maps to get the reachable set $Reach_{\mathcal{A}}$ of \mathcal{A} . This method accelerated the computation of $Reach_{\mathcal{A}}$ since the computation of $Reach_{\mathcal{A}_v}$ reaches a fixed point faster than the former, and transforming reachable sets is cheaper than computing them. However, expectedly, this approach for $Reach_{\mathcal{A}}$ computation results in larger over-approximation errors than computing it directly using existing methods, which limits its usability in safety verification. An example is shown in Figure 1c. Therefore, there is a need for a method that culminates the acceleration benefits of abstraction without trading off accuracy. Another limitation of symmetry abstractions is their requirement for symmetric continuous dynamics. For closed-loop control systems, although the open-loop dynamics might be symmetric, as that of a quadrotor or a car, their controllers might not be. In particular, vehicle controllers are increasingly developed using machine learning approaches like DNNs, which are nonlinear functions resulting from optimization over non-structured data with no symmetry guarantees. How can symmetry abstractions be employed for such DNN-based control systems?

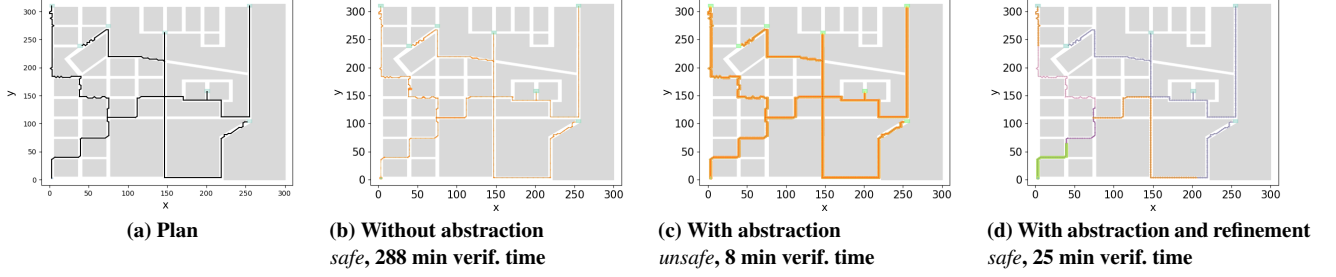


Figure 1: Safety verification of a NN-controlled quadrotor following a planned path of 520 segments in a city using SymAR with DryVR as a reachability computation engine.

In this paper, we present SymAR, a refinement algorithm for symmetry-based abstractions of hybrid automata for fast and accurate safety verification (Algorithm 2). We further propose a method to enforce symmetric properties on non-symmetric controllers by transforming their inputs and outputs with well-chosen maps that match the symmetry of the open-loop dynamics.

Our refinement happens recursively in a depth first search (DFS) manner over the mode graph of the abstraction \mathcal{A}_v of \mathcal{A} . When an abstract mode p_v is being visited, its reachable set is computed using any of the existing reachability tools (e.g. Verisig [14], Sherlock [8], DryVR [10]). If it is unsafe, p_v is split into two modes, each representing half of the modes of \mathcal{A} that were represented by p_v . If that split is not possible, i.e. p_v represents a single mode of \mathcal{A} , the parent of p_v in DFS gets split instead.

The splitting of modes during DFS changes \mathcal{A}_v and its mode graph, complicating the search problem. For example, a cache saving the reachable sets computed for each mode of \mathcal{A}_v usually gets maintained for fixed point checking purposes. Upon a mode split, some of the cached reachable sets of its parent and siblings modes in the DFS graph need to be carefully deleted and recomputed. We tackled this and similar problems in SymAR while avoiding unnecessary repetitions of computations.

We implemented our abstraction refinement-based safety verification method SymAR in Python along with the transformations for making a non-symmetric controller symmetric. We tested it on the NN-controlled quadrotor presented in [14] and also a car that we trained ourselves. We considered complex 2D and 3D scenarios with paths consisting of 100s of segments. Our results show significant acceleration in verification time over existing methods, as that of Figure 1d, while maintaining the accuracy of the result.

2 MODEL AND PROBLEM STATEMENT

Notations. We denote by \mathbb{N} , \mathbb{R} , and $\mathbb{R}^{\geq 0}$ the sets of natural numbers, real numbers and non-negative reals. Given a finite set S , its cardinality is denoted by $|S|$. Given a function $\gamma: \mathbb{R}^k \rightarrow \mathbb{R}^k$ and a set $S \subseteq \mathbb{R}^k$, we abuse notation and define $\gamma S = \{\gamma x \mid x \in S\}$.

2.1 Hybrid automaton

In this section, we present the general definition of hybrid automata that we will use in this paper [2, 15, 17], along with the safety verification problem.

Definition 2.1. A hybrid automaton is a tuple

$$\mathcal{A} := \langle \mathcal{X}, \mathcal{P}, \Theta, p_{init}, E, guard, reset, f \rangle, \text{ where} \quad (1)$$

- (a) $\mathcal{X} \subseteq \mathbb{R}^n$ is the continuous state space, or simply the *state* space, and $\mathcal{P} \subseteq \mathbb{R}^d$ is the discrete state space, which we call the *parameter* or *mode* space,
- (b) $\langle \Theta, p_{init} \rangle \subseteq \mathcal{X} \times \mathcal{P}$ is a pair of a compact set of possible initial states and an initial mode,
- (c) $E \subseteq \mathcal{P} \times \mathcal{P}$ is a set of edges that specify possible transitions between modes,
- (d) $guard: E \rightarrow 2^{\mathcal{X}}$ defines the set of states at which a mode transition over an edge is possible,
- (e) $reset: \mathcal{X} \times E \rightarrow 2^{\mathcal{X}}$ defines the possible updates of the state after a mode transition over an edge, and
- (f) $f: \mathcal{X} \times \mathcal{P} \rightarrow \mathcal{X}$ is the *dynamic* function that define the continuous evolution of the state in each mode. It is Lipschitz continuous in the first argument.

A trajectory $\xi: \mathcal{X} \times \mathcal{P} \times \mathbb{R}^{\geq 0} \rightarrow \mathcal{X}$ of \mathcal{A} starting from initial state x in mode p should satisfy the differential equation:

$$\frac{d\xi}{dt} x, p, t = f \xi x, p, t, p, \quad (2)$$

for any $t \in \mathbb{R}^{\geq 0}$ and $\xi x, p, 0 = x$. For a time bounded trajectory, we denote its duration by $dur \xi$, its initial state by $\xi.fstate$ and last one by $\xi.lstate$.

An execution $\sigma := \xi_0, p_0, \xi_1, p_1, \dots$ of \mathcal{A} is a sequence of pairs of trajectories and modes that have the following properties:

- (1) $\xi_0.fstate \in \Theta, p_0 \in p_{init}, p_i, p_{i+1} \in E$,
- (2) $\xi_i.lstate \in guard p_i, p_{i+1}$, and
- (3) $\xi_{i+1}.fstate \in reset \xi_i.lstate, p_i, p_{i+1}$.

The set of all executions of \mathcal{A} is denoted by $Execs_{\mathcal{A}}$. The set of *reachable states* $Reach_{\mathcal{A}}$ of \mathcal{A} is the set of states reachable by \mathcal{A} . Formally, $Reach_{\mathcal{A}} := \{x \in \mathcal{X} \mid \sigma \in Execs_{\mathcal{A}}, \sigma.lstate = x\}$. When we restrict the states to be those visited in mode p , we denote the reachset by $Reach_{\mathcal{A}} p$.

Given an unsafe map $\mathbf{O}: \mathcal{P} \rightarrow 2^{\mathcal{X}}$, that defines the unsafe set of states in each mode, the *safety verification* problem is to check if $\forall p \in \mathcal{P}$,

$$Reach_{\mathcal{A}} p \cap \mathbf{O} p = \emptyset.$$

2.2 NN-controlled quadrotor case study

In this section, we will describe a case study of a scenario having a planner, NN controller, and a quadrotor and model it as a hybrid automaton. We use the quadrotor model that was presented in [14] along, its trained NN controller, and a RRT planner to construct its reference trajectories, independent of its dynamics.

The dynamics of the quadrotor are as follows:

$$q := \begin{bmatrix} p_x^q \\ p_y^q \\ p_z^q \\ v_x^q \\ v_y^q \\ v_z^q \end{bmatrix} = \begin{bmatrix} v_x^q \\ v_y^q \\ v_z^q \\ g \tan \theta \\ -g \tan \phi \\ \tau - g \end{bmatrix}, w := \begin{bmatrix} p_x^w \\ p_y^w \\ p_z^w \\ v_x^w \\ v_y^w \\ v_z^w \end{bmatrix} = \begin{bmatrix} b_x \\ b_y \\ b_z \\ 0 \\ 0 \\ 0 \end{bmatrix}, \quad (3)$$

where q and w are the states of the quadrotor and the planner reference trajectory representing their position and velocity vectors in the 3D physical space, respectively. The variables θ , ϕ , and τ represent the control inputs pitch, roll, and thrust, respectively, provided by the NN controller. The input to the NN controller is the difference between the quadrotor state and the reference trajectory: $q - w$. The $g = 9.81 \text{ms}^{-2}$ is gravity and b_x, b_y , and b_z are piece-wise constant resulting in a piece-wise linear planner trajectory. In our case, these would be determined by the RRT planner as we will explain next.

The NN controller has two hidden layers with 20 neurons each with \tanh activation units and a linear output layer. It acts as a classifier to choose from a set $\mathbf{U} \subset [-0.1, 0.1] \times [-0.1, 0.1] \times [7.81, 11.81]$ of eight possible control inputs. It was trained to mimic a model predictive control (MPC) controller to drive the quadrotor to follow the planner trajectory. A NN is used for its faster runtime computation and reachability analysis and smaller memory requirements than traditional MPC controllers.

Given an initial set of positions $K \subset \mathbb{R}^3$, a goal set of positions $\mathbf{G} = \cup_i \mathbf{G}_i \subset \mathbb{R}^3$, and a set of 3D obstacles, the planner would generate a directed graph over \mathbb{R}^3 that connects K to every \mathbf{G}_i with piece-wise linear paths. We denote the set of linear segments in the graph by $\mathbf{R} := \{r_i\}_i$. The planner ensures that the waypoints and segments do not intersect obstacles, but without regard of the quadrotor dynamics.

We model such a scenario as a hybrid automaton:

- (a) $\mathcal{X} = \mathbb{R}^6$, the space in which the state of the quadrotor q lives, and $\mathcal{P} = \mathbf{R}$, the space in which the graph segments live, where the first three and last three coordinates determine the start and end points $p.\text{src}$ and $p.\text{dest}$ of the segment, respectively,
- (b) $\langle \Theta, p_{\text{init}} \rangle := \langle K, [-0.5, 0.5]^3, p_{\text{init}} \rangle$, where $[-0.5, 0.5]^3$ are the range of initial velocities of the quadrotor and p_{init} is the initial segment going out of K ,
- (c) $E := \{r_i, r_{i1} \mid r_i, r_{i1} \in \mathbf{R}, r.\text{dest} = r_{i1}.\text{src}\}$,
- (d) $\text{guard}_{r_i, r_{i1}}$ is the 6D ball centered at $r_i.\text{dest}, 0, 0, 0$ with radius $1, 1, 1, \infty, \infty, \infty$, meaning that the quadrotor should arrive within distance 1 unit of the destination waypoint of the first segment, which is equivalent to the source waypoint of the second segment, at any velocity, to be able to transition to the second segment/mode,
- (e) $\text{reset}_{q, r_i, r_{i1}} = q$, meaning that there is no change in the quadrotor state after it starts following a new segment, and
- (f) $f_q, r = gq, hq, r_i$, where $g : \mathcal{X} \times \mathbf{U} \rightarrow \mathcal{X}$ is the right hand side of the differential equation of q in equation (3) and $h : \mathcal{X} \times \mathcal{P} \rightarrow \mathbf{U}$ is the NN controller. Without loss of generalization, we assume that $b_x, b_y, b_z \in \{-0.125, 0.125\}^3$. b_x is equal to -0.125 if $r.\text{src}_0 > r.\text{dest}_0$ and 0.125 otherwise. The same applies for b_y and b_z .

Note that since the NN controller is sampled periodically, and held constant between samples, the control is piece-wise constant.

Such a control might violate the differentiability of f in equation (2), however the solutions still exist and are unique.

3 SYMMETRY AND EQUIVARIANT DYNAMICAL SYSTEMS

Symmetries of dynamical systems are maps acting on their state spaces that transform their trajectories to other trajectories, reducing their analysis complexity. In this section, we present the basic definitions and theorems on symmetries of parameterized dynamical systems. Moreover, we present conditions that feedback controllers should satisfy for a closed loop system to possess certain symmetry.

3.1 Symmetries of dynamical systems

First, let Γ be a group of smooth maps acting on \mathcal{X} .

Definition 3.1 (Definition 2 in [19]). We say that $\gamma \in \Gamma$ is a symmetry of system (2) if its differentiable, invertible, and for any solution $\xi_{x_0}, p, \cdot, \gamma \xi_{x_0}, p, \cdot$ is also a solution.

Coupled with the notion of symmetries, is the notion of equivariant dynamical systems.

Definition 3.2 ([19]). The dynamic function $f : \mathcal{X} \times \mathcal{P} \rightarrow \mathcal{X}$ is said to be Γ -equivariant if for any $\gamma \in \Gamma$, there exists $\rho : \mathcal{P} \rightarrow \mathcal{P}$ such that,

$$\forall x \in \mathcal{X}, \forall p \in \mathcal{P}, \frac{\partial \gamma}{\partial x} f x, p = f \gamma x, \rho p. \quad (4)$$

The following theorem draws the relation between symmetries and equivariance definitions.

THEOREM 3.3 (THEOREM 10 IN [19]). *If f is Γ -equivariant, then all maps in Γ are symmetries of (2). Moreover, for any $\gamma \in \Gamma$, map $\rho : \mathcal{P} \rightarrow \mathcal{P}$ that satisfies equation (4), $x_0 \in \mathcal{X}$, and $p \in \mathcal{P}$, $\gamma \xi_{x_0}, p, \cdot = \xi_{\gamma x_0}, \rho p, \cdot$.*

That means that one can get the trajectory of the system starting from an initial state γx_0 in mode ρp by transforming its trajectory starting from x_0 in mode p using γ .

3.2 Symmetries of closed loop control systems

In this section, we will consider the special case when the dynamical system in equation (2) is a closed loop control system similar to that of the quadrotor formalized in part (f) of its hybrid automaton definition in Section 2.2. Mainly, we discuss the property that the controller should satisfy for the system to be symmetric.

Fix an input space $\mathbf{U} \subseteq \mathbb{R}^m$ and consider a right hand side of equation (2) of the form:

$$f_c x, p := g x, h x, p, \quad (5)$$

where $g : \mathcal{X} \times \mathbf{U} \rightarrow \mathcal{X}$ and $h : \mathcal{X} \times \mathcal{P} \rightarrow \mathbf{U}$ are Lipschitz continuous functions with respect to both of their arguments.

In order to retain symmetry for such systems, we update the notion of equivariance of dynamic functions. But first, let us define symmetric controllers.

Definition 3.4. Given three maps $\beta : \mathbf{U} \rightarrow \mathbf{U}$, $\gamma : \mathcal{X} \rightarrow \mathcal{X}$, and $\rho : \mathcal{P} \rightarrow \mathcal{P}$. We call the control function h, β, γ, ρ -symmetric, if for all $x \in \mathcal{X}$ and $p \in \mathcal{P}$, $\beta h x, p = h \gamma x, \rho p$.

Definition 3.4 means that if we transform the input of the controller, the state and the mode, using the maps γ and ρ , respectively, then its output gets transformed with the map β . Such a property formalizes intuitive assumptions about controllers in general. For example, translating the position of the quadrotor and the planned trajectory by the same vector should not change the controller output. The NN controller discussed in Section 2.2 indeed satisfies this property since its input is the relative state $q - w$. We update the notion of equivariance for closed-loop control systems to account for the controller in the following definition.

Definition 3.5. We call the control system dynamic function f_c of equation (5) Γ -equivariant if for any $\gamma \in \Gamma$, there exist $\rho : \mathcal{P} \rightarrow \mathcal{P}$ and $\beta : \mathcal{U} \rightarrow \mathcal{U}$ such that h is β, γ, ρ -symmetric and

$$\forall x \in \mathcal{X}, \forall u \in \mathcal{U}, \frac{\partial \gamma}{\partial x} g x, u = g \gamma x, \beta u. \quad (6)$$

The following theorem repeats the results of Theorem 3.3 for the closed loop control system.

THEOREM 3.6. If f_c of equation (5) is Γ -equivariant, then all maps in Γ are symmetries. Moreover, for any $\gamma \in \Gamma$, maps $\rho : \mathcal{P} \rightarrow \mathcal{P}$ and $\beta : \mathcal{U} \rightarrow \mathcal{U}$ that satisfy equation (6), $x_0 \in \mathcal{X}$, and $p \in \mathcal{P}$, $\gamma \xi_c x_0, p, \cdot = \xi_c \gamma x_0, \rho p, \cdot$, where ξ_c is the trajectory of the dynamical system with RHS equation (5).

PROOF. Fix an initial state $x_0 \in \mathcal{X}$, a mode $p \in \mathcal{P}$, and $\gamma \in \Gamma$ with its corresponding maps ρ and β that satisfy Definition 3.2 per the assumption of the theorem. For any $t \geq 0$, let $x = \xi_c x_0, p, t$ and $y = \gamma x$. Then,

$$\begin{aligned} \frac{dy}{dt} &= \frac{\partial \gamma}{\partial x} \frac{dx}{dt}, \text{ using the chain rule,} \\ &= \frac{\partial \gamma}{\partial x} g x, h x, p, \text{ using equation (5),} \\ &= g \gamma x, \beta h x, p, \text{ using equation (6),} \\ &= g \gamma x, h \gamma x, \rho p, \text{ using Definition 3.4,} \\ &= g y, h y, \rho p, \text{ by substituting } \gamma x \text{ with } y, \\ &= f_c y, \rho p. \end{aligned} \quad (7)$$

Hence, $\gamma \xi_c x_0, p, t$ also satisfies equation (5) and thus a valid solution of the system. Therefore, γ is a symmetry per Definition 3.1. Moreover, y is a solution starting from γx_0 in mode ρp . This proof is similar to that of Theorem 10 in [19] with is the difference of having a controller h , which requires the additional assumption that h is symmetric. \square

In Section 5, we discuss how to make non-symmetric controllers symmetric, and apply that to the NN-controller of the quadrotor to make it rotation symmetric.

4 REFINEMENT OF SYMMETRY-BASED ABSTRACTION OF HYBRID AUTOMATA

In this section, we present our refinement algorithm SymAR of symmetry abstractions.

4.1 Abstraction definition

The abstraction in [20] requires a set of symmetry maps which they call the *virtual map*, defined as follows:

Definition 4.1 (Definition 4 in [20]). Given a hybrid automaton \mathcal{A} , a virtual map is a set

$$\Phi = \{\gamma_p, \rho_p\}_{p \in P}, \quad (8)$$

where for every $p \in P$, $\gamma_p : \mathcal{X} \rightarrow \mathcal{X}$, $\rho_p : \mathcal{P} \rightarrow \mathcal{P}$, and they satisfy equation (4).

Given a virtual map Φ , they define a new map $rv : \mathcal{P} \rightarrow \mathcal{P}$ as follows: $rvp = \rho_p p$. It maps modes of the original automaton \mathcal{A} to their corresponding ones in the abstract one \mathcal{A}_v , defined next.

The idea of the abstraction is to group modes of \mathcal{A} that share similar behavior in symmetry terms together in the same mode in the abstract automaton. The trajectories of such modes can be obtained by transforming the trajectories of the corresponding abstract mode using symmetry maps.

Definition 4.2 (Definition 5 in [20]). Given a hybrid automaton \mathcal{A} , and a virtual map Φ , the resulting *abstract (virtual) hybrid automaton* is:

$$\mathcal{A}_v = \langle \mathcal{X}_v, \mathcal{P}_v, \Theta_v, p_{init,v}, E_v, guard_v, reset_v, f_v \rangle, \text{ where}$$

- (a) $\mathcal{X}_v = \mathcal{X}$ and $\mathcal{P}_v = rv\mathcal{P}$
- (b) $X_{init,v} = \gamma_{p_{init}} \Theta$ and $p_{init,v} = rv p_{init}$,
- (c) $E_v = rv E = \{rv p_1, rv p_2 \mid e = p_1, p_2 \in E\}$
- (d) $\forall e_v \in E_v$,

$$guard_v e_v = \bigwedge_{e \in rv^{-1} e_v} \gamma_{e.src} (guard_e),$$

- (e) $\forall x_v \in \mathcal{X}_v, e_v \in E_v$,

$$reset_v x_v, e_v = \bigwedge_{e \in rv^{-1} e_v} \gamma_{e.dest} (reset(\gamma_{e.src}^{-1} x_v, e)), \text{ and}$$

- (f) $\forall p_v \in \mathcal{P}_v, \forall x \in \mathcal{X}, f_v x, p_v = f x, p_v$.

4.2 Quadrotor abstract automaton

An example virtual map of the quadrotor in Section 2.2 would be the one that has for any mode r , i.e. waypoint segment, ρ_r , which maps it to the mode r_v , that is of same length as r but aligned with the y -axis and has its end point at the origin. Additionally, it would have γ_r being the map that transforms the state to the new coordinate system of the physical space. Such a map would result in an abstract automaton where all segments of \mathbf{R} having the same length and same relative z -distance between their end points being mapped to the same abstract mode. For more elaborate construction of similar abstractions, the reader is referred to [20]. In this section, we assumed that the controller is symmetric, which is not, and we will tackle this issue in Section 5.

4.3 Forward simulation relations

For an automaton \mathcal{A}_1 to be an abstraction of another one \mathcal{A}_2 , a forward simulation relation (FSR) is usually defined to show that for any execution of \mathcal{A}_2 , there is a corresponding one of \mathcal{A}_1 that represents it. The following is a formal definition of FSR.

Definition 4.3 ([15]). A forward simulation relation from hybrid automaton \mathcal{A}_1 to another one \mathcal{A}_2 , is a relation $\mathcal{R} \subseteq \mathcal{X}_1 \times \mathcal{P}_1 \times \mathcal{X}_2 \times \mathcal{P}_2$, such that

- (a) for any initial state $x_1 \in \Theta_1$, there exists a state $x_2 \in \Theta_2$, such that $x_1, p_{init,1} \mathcal{R} x_2, p_{init,2}$,

- (b) for any discrete transition $x_1, p_1 \rightarrow x'_1, p'_1$ of \mathcal{A}_1 and $x_2, p_2 \in \mathcal{X}_2 \times \mathcal{P}_2$, where $x_1, p_1 \mathcal{R} x_2, p_2$, there exists $x'_2, p'_2 \in \mathcal{X}_2 \times \mathcal{P}_2$ such that $x_2, p_2 \rightarrow x'_2, p'_2$ is a discrete transition of \mathcal{A}_2 and $x'_1, p'_1 \mathcal{R} x'_2, p'_2$, and
- (c) for any solution $\xi_1 x_1, p_1, \cdot$ of \mathcal{A}_1 and pair x_2, p_2 , such that $x_1, p_1 \mathcal{R} x_2, p_2$, there exists a solution $\xi_2 x_2, p_2, \cdot$ of \mathcal{A}_2 , with $\text{dur}\xi_1 = \text{dur}\xi_2$ and $\xi_1.\text{lstate}, p_1 \mathcal{R} \xi_2.\text{lstate}, p_2$.

The implication of the existence of a FSR on the relation between the trajectories of the two automata is formalized in the following theorem from [20], which is a modified version of Corollary 4.23 of [15] for the hybrid automaton of Definition 2.1.

THEOREM 4.4 ([15]). *If there exists a forward simulation relation \mathcal{R} from \mathcal{A}_1 to \mathcal{A}_2 , then for every execution σ_1 of \mathcal{A}_1 , there exists a corresponding execution σ_2 of \mathcal{A}_2 such that*

- (a) $\sigma_1.\text{len} = \sigma_2.\text{len}$,
- (b) $\forall i \in \sigma_1.\text{len}, \text{dur}\xi_{1,i} = \text{dur}\xi_{2,i}$, and
- (c) $\forall i \in \sigma_1.\text{len}, \xi_{1,i}.\text{lstate}, p_{1,i} \mathcal{R} \xi_{2,i}.\text{lstate}, p_{2,i}$.

If there exists a FSR \mathcal{R} from \mathcal{A}_1 to \mathcal{A}_2 , we say that $\mathcal{A}_1 \preceq_{\mathcal{R}} \mathcal{A}_2$. A FSR has been suggested in [20] from the automaton \mathcal{A} of Definition 2.1 to \mathcal{A}_v , that of Definition 4.2.

THEOREM 4.5 (THEOREM 3 IN [20]). *Consider the relation $\mathcal{R}_{rv} \subseteq \mathcal{X} \times \mathcal{P} \times \mathcal{X}_v \times \mathcal{P}_v$ defined as $x, p \mathcal{R}_{rv} x_v, p_v$ if and only if:*

- (a) $x_v = \gamma_p x$, and
- (b) $p_v = rv p$.

Then, \mathcal{R}_{rv} is a forward simulation relation from \mathcal{A} to \mathcal{A}_v .

4.4 Safety verification of the abstract automaton

In this paper, we map the unsafe map \mathbf{O} of \mathcal{A} to the abstract automaton \mathcal{A}_v . It will be used later in the safety verification algorithm in Section 4.6. We define for every $p_v \in \mathcal{P}_v$,

$$\mathbf{O}_v p_v := \bigcup_{rv^{-1}p_v} \gamma_p \mathbf{O} p. \quad (9)$$

The following theorem on the relation between the safety of \mathcal{A} with respect to \mathbf{O} and \mathcal{A}_v with respect to \mathbf{O}_v follows from the FSR in the previous theorem.

THEOREM 4.6. *Fix any $p \in \mathcal{P}$ and let $p_v = rv p$. If $\text{Reach}_{\mathcal{A}} p \cap \mathbf{O} p \neq \emptyset$, then $\text{Reach}_{\mathcal{A}_v} p_v \cap \mathbf{O}_v p_v \neq \emptyset$.*

The theorem above shows that if \mathcal{A} is unsafe, then \mathcal{A}_v is unsafe as well. The converse is not necessarily true since \mathcal{A}_v might have executions that do not correspond to ones of \mathcal{A} .

4.5 Abstraction refinement by splitting modes

In this section, we describe `splitMode`, the algorithm used to split an abstract mode p_v^* and update the abstract automaton \mathcal{A}_v . Then, we prove that its result \mathcal{A}'_v is an abstraction of \mathcal{A} and that \mathcal{A}_v is an abstraction of \mathcal{A}'_v , using two forward simulation relations.

4.5.1 splitMode description. The procedure `splitMode` takes as input the mode to be split p_v^* , the map rv that maps original modes to abstract ones, the original and abstract automata \mathcal{A} and \mathcal{A}_v , and the original and abstract unsafe maps \mathbf{O} and \mathbf{O}_v . It outputs the two resulting modes $p_{v,1}$ and $p_{v,2}$ of the splitting of p_v^* , the updated map rv , updated abstract automaton \mathcal{A}_v , the updated abstract unsafe map \mathbf{O}'_v , and a boolean indicating if the splitting was successful.

It starts by obtaining the set of original modes P of \mathcal{A} represented by p_v^* in line 2. If the number of these modes is less than two, then the algorithm returns the given input along with a *False* flag to indicate failure to split in line 3. Otherwise, it initializes the output variables rv' , \mathcal{A}'_v , and \mathbf{O}'_v by copying rv , \mathcal{A}_v , and \mathbf{O}_v . It then creates two new abstract modes $p_{v,1}$ and $p_{v,2}$ and adds them to \mathcal{P}'_v in line 5. Then, it decomposes P into two disjoint sets P_1 and P_2 , in line 6. After that, it updates the map rv to map modes in P_1 to $p_{v,1}$ and those of P_2 to $p_{v,2}$ in line 7. It then updates the initial mode of \mathcal{A}'_v in case the split mode was the root.

Now that it created the new modes, it proceeds into updating the edges of \mathcal{A}'_v and their *guard* _{v} and *reset* _{v} annotations. It iterates over the edges that connect p_v^* with its *parents*, which may include p_v^* itself, and create for each such edge, two edges connecting that parent with both $p_{v,1}$ and $p_{v,2}$ in line 9. It repeats the same process but for the edges that connect p_v^* with its *children* in line 11. Finally, it checks if p_v^* had an edge connecting it to itself, and if that is the case, creates two edges connecting each of $p_{v,1}$ and $p_{v,2}$ to themselves.

In line 15, it annotates the created edges with their guards and resets in the same way Definition 4.2 defined them, but using the update map rv' . In lines 17 and 18, it sets the dynamic function of both modes to be the same as that of p_v^* . Finally, it deletes p_v^* with all edges connected to it in line 19. It then initializes the unsafe maps for the newly created modes by decomposing the unsafe set of p_v^* into those of the two modes. It returns in line 22 the new modes, new rv' and \mathcal{A}'_v , the unsafe map \mathbf{O}'_v , and the flag *True* to indicate successful splitting.

Algorithm 1 `splitMode`

```

1: input:  $p_v^*, rv, \mathcal{A}, \mathcal{A}_v, \mathbf{O}, \mathbf{O}_v$ 
2:  $P \leftarrow rv^{-1} p_v^*$ .
3: if  $|P| < 2$  then return:  $\perp, \perp, rv, \mathcal{A}_v, \mathbf{O}_v, \text{False}$ .
4: Create copies of  $rv$ ,  $\mathcal{A}_v$ , and  $\mathbf{O}_v$ , and name them  $rv'$ ,  $\mathcal{A}'_v$ , and  $\mathbf{O}'_v$ .
5: Create two new virtual modes  $p_{v,1}$  and  $p_{v,2}$  and add them to  $\mathcal{P}'_v$ .
6: Split  $P$  in half to two sets  $P_1$  and  $P_2$ .
7:  $rv' P_1 \leftarrow p_{v,1}$ ,  $rv' P_2 \leftarrow p_{v,2}$ .
8:  $p'_{init,v} \leftarrow rv' p_{init}$ 
9: for  $e_v \in E_v$  such that  $e_v.\text{dest} = p_v^*$  do
10:   Create two new edges  $e_v.\text{src}, p_{v,1}$  and  $e_v.\text{src}, p_{v,2}$ .
11: for  $e_v \in E_v$  such that  $e_v.\text{src} = p_v^*$  do
12:   Create two new edges  $p_{v,1}, e_v.\text{dest}$  and  $p_{v,2}, e_v.\text{dest}$ .
13: if  $\exists e_v \in E_v$  such that  $e_v.\text{src} = e_v.\text{dest} = p_v^*$  then
14:   Create two new edges  $p_{v,1}, p_{v,1}$  and  $p_{v,2}, p_{v,2}$ .
15: Define the guards and resets of new edges using the virtual map  $rv'$ .
16: Remove added edges that have empty guards.
17: Set  $f'_{v,1}, p_{v,1} = f_v, p_v^*$ .
18: Set  $f'_{v,2}, p_{v,2} = f_v, p_v^*$ .
19: Remove  $p_v^*$  from  $\mathcal{P}'_v$  and  $\mathbf{O}'_v$ , and remove all attached edges from  $E'_v$ .
20:  $\mathbf{O}'_v p_{v,1} \leftarrow \bigcup_{p \in P_1} \gamma_p \mathbf{O}_v p$ 
21:  $\mathbf{O}'_v p_{v,2} \leftarrow \bigcup_{p \in P_2} \gamma_p \mathbf{O}_v p$ 
22: return:  $p_{v,1}, p_{v,2}, rv', \mathcal{A}'_v, \mathbf{O}'_v, \text{True}$ 

```

4.5.2 Correctness guarantees of `splitMode`. In this section, we show that the resulting automaton \mathcal{A}'_v from `splitMode` is still a valid abstraction of \mathcal{A} , but it is a tighter one than \mathcal{A}_v by showing that \mathcal{A}_v is an abstraction of \mathcal{A}'_v .

Consider $\mathcal{R}_{rv'}$, the same relation as \mathcal{R}_{rv} defined in Theorem 4.5, but using rv' instead of rv . Formally, $\mathcal{R}_{rv'} \subseteq \mathcal{X} \times \mathcal{P} \times \mathcal{X}'_v \times \mathcal{P}'_v$ defined as $x, p \mathcal{R}_{rv'} x'_v, p'_v$ if and only if:

- (a) $x'_v = \gamma_p x$, and
- (b) $p'_v = rv' p$.

Let us refer to $\mathcal{R}_{rv'}$ by \mathcal{R}_1 and let $\mathcal{R}_2 \subseteq \mathcal{X}'_v \times \mathcal{P}'_v \times \mathcal{X}_v \times \mathcal{P}_v$ be defined as: $x'_v, p'_v \mathcal{R}_2 x_v, p_v$ if and only if:

- (a) $x_v = x'_v$, and
- (b)

$$p_v = \begin{cases} p'_v, & \text{if } p'_v \notin \{p_{v,1}, p_{v,2}\}, \\ p_v^*, & \text{otherwise.} \end{cases} \quad (10)$$

The following theorem shows that these two relations are forward simulation relations between \mathcal{A} and \mathcal{A}'_v and \mathcal{A}'_v and \mathcal{A}_v , respectively.

THEOREM 4.7. *Fix any abstract mode $p_v^* \in \mathcal{P}_v$ of \mathcal{A}_v and let $rv', \mathcal{A}'_v = \text{splitMode}^*(rv, \mathcal{A}_v)$. Then, the resulting relations \mathcal{R}_1 and \mathcal{R}_2 are FSRs from \mathcal{A} to \mathcal{A}'_v and \mathcal{A}'_v to \mathcal{A}_v , respectively, and $\mathcal{A} \preceq_{\mathcal{R}_1} \mathcal{A}'_v \preceq_{\mathcal{R}_2} \mathcal{A}_v$.*

PROOF. Let us prove the first half first: that \mathcal{R}_1 is a FSR from \mathcal{A} to \mathcal{A}'_v . We do that by showing that \mathcal{A}'_v is the result of following Definition 4.2 to create an abstraction of \mathcal{A} using a slightly modified version Φ' of the virtual map Φ , where Φ' itself is another virtual map for \mathcal{A} .

By definition, $\forall p \in \mathcal{P}, rv p = \rho_p p$, where $\gamma_p, \rho_p \in \Phi$. Let Φ' be equal to Φ for all $p \notin P$, where P is as in line 2 of `splitMode`. For any $p \in P$, let $\rho'_p p = p_{v,1}$, if $p \in P_1$, and $\rho'_p p = p_{v,2}$, otherwise. Moreover, as in lines 17 and 18, define the continuous dynamics f'_v to be equal to f_v , for all $p_v \in \mathcal{P}_v \setminus \{p_{v,1}, p_{v,2}\}$, and to be equal to $f_v \cdot p_v^*$, otherwise. Then, Φ' is a virtual map of f'_v since any $\gamma'_p, \rho'_p \in \Phi'$ satisfies equation (4) for f'_v , because the corresponding $\gamma_p, \rho_p \in \Phi$ satisfies it for f_v . The map rv' is just the result of Φ' as rv is the result of Φ .

The edges created in `splitMode` for $p_{v,1}$ and $p_{v,2}$ in \mathcal{A}'_v are a decomposition of the edges connected to p_v^* in \mathcal{A}_v , including self edges. Hence, the output of `splitMode` \mathcal{A}'_v is indeed the result of following Definition 4.2 to construct an abstraction of \mathcal{A} using rv' . It follows from Theorem 4.5, that \mathcal{A}'_v is an abstraction of \mathcal{A} and $\mathcal{R}_1 = \mathcal{R}_{rv'}$ is a corresponding FSR.

Now we prove the second half of the theorem: that \mathcal{R}_2 is a FSR from \mathcal{A}'_v to \mathcal{A}_v . We follow similar steps of the proof of the first half in defining a new map, which we name Φ_2 , and prove that it is a virtual map of \mathcal{A}'_v . Let $\Phi_2 = \{\gamma_{p'_v}, \rho_{p'_v}\}_{p'_v \in \mathcal{P}'_v}$, where $\gamma_{p'_v} x'_v = x'_v$ is the identity map and $\rho_{p'_v} p'_v = p'_v$, if $p'_v \notin \{p_{v,1}, p_{v,2}\}$, and $\rho_{p'_v} p'_v = p_v^*$, otherwise. Because of lines 17 and 18, $\gamma_{p'_v}, \rho_{p'_v}$ satisfy equation (4) with the RHS dynamic function being f'_v of f . Finally, notice that \mathcal{A}_v can be retrieved from \mathcal{A}'_v by following Definition 4.2 using Φ_2 . It follows from Theorem 4.5, that \mathcal{R}_2 is a FSR from \mathcal{A}'_v to \mathcal{A}_v . Thus, $\mathcal{A} \preceq_{\mathcal{R}_1} \mathcal{A}'_v \preceq_{\mathcal{R}_2} \mathcal{A}_v$. \square

REMARK 1. *If in `splitMode`, instead of removing p_v^* from \mathcal{P}'_v with all of its connected edges, p_v^* is kept with only its outgoing edges, it will not be visited by any execution of \mathcal{A}'_v , and the correctness guarantees of `splitMode` would not be altered. This version will be used in the safety verification algorithm in Section 4.6. If p_v^* has a self edge e_v , we delete it and create two outgoing edges from p_v^* to*

$p_{v,1}$ and $p_{v,2}$, with guards and resets being the parts of guard and reset of e_v that correspond to modes in P_1 and P_2 .

4.5.3 Usefulness of `splitMode` in safety verification. We discuss now the benefits of splitting a mode p_v^* , where $\text{Reach}_{\mathcal{A}_v} p_v^* \cap \mathbf{O}_v p_v^* \neq \emptyset$. The non-empty intersection with the unsafe set can mean either that:

- (1) *genuine counterexample*: $\exists p \in \mathcal{P}$ of \mathcal{A} where $\text{Reach}_{\mathcal{A}} p \cap \mathbf{O} p \neq \emptyset$, and thus \mathcal{A} is unsafe, or
- (2) *spurious counterexample*: there exists an execution of \mathcal{A}_v that does not correspond to a one of \mathcal{A} that is intersecting $\mathbf{O}_v p_v^*$, and thus the intersection is a result of the abstraction, and not a correct counterexample.

Spurious counter examples could happen because of the guards and resets of the edges incoming to p_v^* being too large that the initial set of states for that mode is being larger than it should. Remember from Definition 4.2, that the guard and reset of any of these edges e_v is the union of all the transformed guards and resets of the edges in E that get mapped to e_v . If too many of the original edges are mapped to e_v , its guard and reset will get larger, causing more transitions and larger initial set of p_v^* in \mathcal{A}_v . This might increase the possibility of spurious counter example. Moreover, from equation (9), $\mathbf{O}_v p_v$ is the union of the unsafe sets of all the modes that are mapped to p_v^* under rv . The more the original modes that get mapped to p_v^* , the larger is the unsafe set of p_v^* and the higher is the chance of a spurious counter example.

Upon splitting p_v^* into two abstract modes, the guards of the edges incoming to p_v^* , i.e. where p_v^* is a destination, will have their guards divided between the edges to $p_{v,1}$ and $p_{v,2}$. Additionally, the unsafe sets of p_v^* will be divided between $p_{v,1}$ and $p_{v,2}$. This will make the over-approximation of the behaviors of \mathcal{A} by \mathcal{A}_v get tighter and safety checking less conservative. We will discuss how he will use this in a faster, but accurate, solving of the safety verification problem of \mathcal{A} in the next section.

4.6 Abstraction refinement based safety verification algorithm

In [20], it has been suggested to compute the reachset of \mathcal{A}_v of Definition 4.2, without checking safety, while caching the per-mode reachsets in a dictionary. Once a fixed point is reached, they use the symmetry maps in the virtual map Φ to transform the per-mode reachsets of \mathcal{A}_v in the dictionary to get back the per-mode reachsets of \mathcal{A} . Finally, the resulting reachset of \mathcal{A} is intersected with the unsafe set for safety verification. Such an algorithm lacks the flexibility in modifying the abstraction to eliminate the spurious counterexamples automatically, but rather limited by the virtual map given at hand. In this section, we describe how to use `splitMode` to refine \mathcal{A}_v in the process of the safety verification of \mathcal{A} .

Our pseudo code is shown in Algorithm 2, which we denote by `SymAR`. The idea of the algorithm `SymAR` is to compute the reachset of \mathcal{A}_v in the usual way of doing a DFS over the mode graph and computing the reachset of each visited mode till a fixed point is reached. At any particular mode p_v^* being visited, if the computed reachset of p_v^* , or any of the modes in the search subtree starting at p_v^* , is unsafe, `SymAR` calls `splitMode` to split p_v^* into two modes, to eliminate the possibility of spurious counterexample. If p_v^* cannot be refined, `SymAR` would undo the computations done in

that subtree and returns that subtree is unsafe. That would lead one of p_v^* ancestors to be refined, if any could, resulting in a tighter reachset so that when p_v^* is visited again, less spurious counterexample would be possible.

4.6.1 SymAR description. The algorithm SymAR is a recursive function that do depth first search (DFS) over the graph of modes and edges of \mathcal{A}_v . It takes as input \mathcal{A}_v , a mode $p_v^* \in \mathcal{P}_v$ from which we need to continue the reachset computation of \mathcal{A}_v , the parent mode, from which p_v^* has been called, the reachset R_v of $parent$ that has been computed before calling p_v^* , a dictionary storing the per-mode reachsets of all modes in \mathcal{A}_v and their corresponding initial sets, and the unsafe map \mathbf{O}_v . It outputs a new abstract automaton \mathcal{A}_v' that is a refined version of \mathcal{A}_v , a corresponding refined version of the unsafe set \mathbf{O}_v' , an updated dictionary $Cache'$ of $Cache$ that store the reachsets computed for all modes of \mathcal{A}_v' , a dictionary $refree$ that maps all modes of \mathcal{A} to their corresponding refined modes in \mathcal{A}_v' , an indicator $fixedpoint$ if a fixed point has been reached, and an indicator $issafe$ showing if \mathcal{A}_v starting from p_v^* with parent $parent$ of reachset R_v while the per-mode reachsets in the computation of the reachset of \mathcal{A}_v are as stored in $Cache$ is safe with respect to the unsafe map \mathbf{O}_v .

It starts with computing the initial set K_v of p_v^* at this visit in lines 2 to 5. If p_v^* is the root, i.e. the initial mode of \mathcal{A}_v , then $K_v = \Theta_v$, where Θ_v is part of \mathcal{A}_v definition. Otherwise, the parent reachset R_v is intersected with the $guard_v$ of the edge connecting p_v^* 's parent to p_v^* , then reseted using $reset_v$ of the same edge to get K_v . If the reachset starting from K_v in mode p_v^* has been computed before and saved in $Cache$, then no need to explore this subtree again and the flag of fixed point $fixedpoint$, is set to *True*, and SymAR returns *safe* in line 7. Otherwise, reachset computation should be done.

After that, it starts with initializing the *refine* flag to *False*, and the output automaton \mathcal{A}_v' , output unsafe map \mathbf{O}_v' , and reachsets and initial sets dictionary $Cache'$, to the input ones \mathcal{A}_v , \mathbf{O}_v , and $Cache$, respectively (lines 8 and 9). It initializes the dictionary $refree$ to be the modes themselves in line 11. Then, in line 12, the reachset $newR_v$ is computed using the method `computeReachset`, which is a call to any of the existing tools (e.g. Verisig[14], Sherlock [8], NNV [21], DryVR [10], if the system has a NN controller, or flow* [5], C2E2 [7], DryVR [10] otherwise). If the computed reachset intersects the unsafe set, the *refine* is set to *True* and it jumps to line 31. Otherwise, both $newR_v$ and K_v are added to the entry of p_v^* in $Cache'$ in lines 16 and 17. Such an addition is not permanent, it is on-hold till making sure that all the subtree starting from p_v^* is safe as well. The *fixedpoint* flag is initialized to *True* in line 18. If any of the children of p_v^* did not reach fixed point yet, this flag would be set to *False* again in line 23.

At this point, SymAR iterates over all children of p_v^* in \mathcal{A}_v , and not in \mathcal{A}_v' in line 19. For each child mode, SymAR iterates over its set of refined modes in $refree$ in line 20. Such a loop accounts for the case if that child mode has been refined by one of its siblings that has been visited before it by the outer loop. For each mode p_v' looped over in the inner loop, SymAR is called using: the most updated version \mathcal{A}_v' that includes all the refinements of the siblings, and their subtrees, done so far, along with the corresponding refined unsafe map \mathbf{O}_v' and the most updated $Cache'$ that contains all safe reachsets computed so far, with p_v' parent being p_v^* and p_v^* 's reachset

being $newR_v$. All refinements done in that SymAR call, are added to those in $refree$. That means that for each mode p_v' in \mathcal{A}_v' , $refree p_v'$ will have all the modes that has been created by splitting p_v' and its refined modes. If the call of SymAR on p_v' returned *unsafe*, the dictionary $Cache'$, along with \mathcal{A}_v' , \mathbf{O}_v' , rv' , and $refree$ gets reset to the input ones in lines 26, 27, and 28, undoing all computations done since line 12, including those done by the siblings. This is to make sure that $Cache'$ only stores reachsets that are safe and lead to safe execution after p_v^* . After resetting, the *refine* flag is set to *True* and the loop is exited to line 31. If instead all calls to SymAR for p_v^* refined children modes returned *safe*, SymAR would return *safe* along with the refined automaton, unsafe map, dictionary of refined modes, and the fixed point flag in line 49.

If *refine* is *True* at line 31, SymAR proceeds into refining p_v^* . In line 32, `splitMode` is called to split p_v^* . Note that as in Remark 1, we keep p_v^* in \mathcal{A}_v' with only its outgoing edges, only deleting the self edge and creating instead two outgoing edges with corresponding guards and resets. If the split was not successful, SymAR returns *unsafe* in line 34. Otherwise, it updates $refree$ next by replacing p_v^* with $p_{v,1}$ and $p_{v,2}$ in the entry of p_v^* in line 35. It copies the reachset and initial sets dictionary $Cache$ of p_v^* into those of the refined modes $p_{v,1}$ and $p_{v,2}$ in lines 36 and 37. If p_v^* was the root, i.e. $parent = \perp$, SymAR is called with the new root mode of \mathcal{A}_v' obtained after refinement using rv' and it returns the result in line 39. Otherwise, it iterates over the two refined modes of p_v^* , and call SymAR with the same input parent $parent$ and reachset R_v as p_v^* . If any returned *unsafe*, it would return *unsafe* as well.

4.6.2 SymAR soundness and completeness guarantees. Given a hybrid automaton \mathcal{A} , an unsafe map \mathbf{O} , a virtual map Φ with its corresponding map rv , the initial call to SymAR would be:

$$\text{SymAR}rv, \mathcal{A}_v, p_{init,v}, \perp, \emptyset, Cache, \mathbf{O}_v, \quad (11)$$

where \mathcal{A}_v is the result of Definition 4.2, $p_{init,v}$ is its initial mode, \mathbf{O}_v is as equation (9), and $Cache$ is a dictionary mapping every mode in \mathcal{A}_v to an empty set. Two key guarantees SymAR provides: (1) it keeps the correctness of the safety verification algorithm that does not use abstraction intact, i.e. soundness and (2) it provides the same result as it is without using abstraction: if that returns *safe*, then it returns *safe* and vice versa.

It does that by keeping the invariant that the refined automata are abstractions of \mathcal{A} and that each time an automaton is generated by refinement, it is an abstraction for the one it got generated from. More importantly, it keeps a well defined interaction between the different abstractions by making the loop in line 19 iterates over the non-refined modes and let $refree$ handle the boundary between the two abstractions. Finally, for any mode with a reachset intersecting the unsafe set, it keeps refining that mode and its ancestors till safety can be proven or no more refinements are allowed. In the worst case scenario, \mathcal{A}_v can be refined completely to become \mathcal{A} again, resulting in the completeness guarantee. More formal proof will be provided in the longer version of the paper.

THEOREM 4.8 (SOUNDNESS). *If SymAR returned safe for the call in equation (11), then \mathcal{A} is safe with respect to \mathbf{O} .*

THEOREM 4.9 (COMPLETENESS). *Fix \mathcal{A} and \mathbf{O} . If \mathcal{A} is safe with respect to \mathbf{O} , and that can be proven by SymAR if it is given*

Algorithm 2 SymAR

```

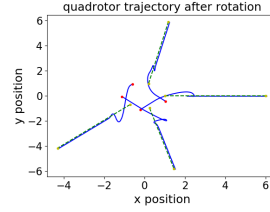
1: input:  $rv, \mathcal{A}_v, p_v^*, parent, R_v, Cache, \mathbf{O}_v$ 
2: if  $parent = \perp$  then  $K_v \leftarrow \Theta_v$ 
3: else
4:    $e_v \leftarrow parent, p_v^*$ 
5:    $grdinter \leftarrow R_v \cap guard_v e_v; K_v \leftarrow reset_v grdinter, e_v$ 
6: if  $K_v \subseteq Cache^*.initset$  then
7:   return:  $\mathcal{A}_v, \mathbf{O}_v, Cache, \{\}, True, safe$ 
8:  $refine \leftarrow False$ 
9:  $\mathcal{A}'_v, \mathbf{O}'_v, rv' \leftarrow copy \mathcal{A}_v, \mathbf{O}_v, rv$ 
10:  $Cache' \leftarrow copy Cache$ 
11:  $refree \leftarrow \{p_v : \{p_v\}\}_{p_v \in \mathcal{P}_v}$ 
12:  $newR_v \leftarrow computeReachset \mathcal{A}_v, K_v, p_v^*$ 
13: if  $newR_v \cap \mathbf{O}_v p_v^* \neq \emptyset$  then
14:    $refine \leftarrow True$ 
15: else
16:    $Cache' p_v^*.reach \leftarrow Cache' p_v^*.reach \cup newR_v$ 
17:    $Cache' p_v^*.initset \leftarrow Cache' p_v^*.initset \cup K_v$ 
18:    $fixedpoint \leftarrow True$ 
19:   for  $e_v \in E_v$  such that  $e_v.src = p_v^*$  do
20:     for  $p'_v \in refree_{e_v}.dest$  do
21:        $rv', \mathcal{A}'_v, \mathbf{O}'_v, Cache', curreftree, curfix, cursafe$ 
22:        $\leftarrow SymAR rv', \mathcal{A}'_v, p'_v, p_v^*, newR_v, Cache', \mathbf{O}'_v$ 
23:       if  $curfix = False$  then  $fixedpoint \leftarrow False$ 
24:        $refree \leftarrow refree \cup curreftree$ 
25:       if  $cursafe = unsafe$  then
26:          $Cache' \leftarrow copy Cache$ 
27:          $\mathcal{A}'_v, \mathbf{O}'_v, rv' \leftarrow copy \mathcal{A}_v, \mathbf{O}_v, rv$ 
28:          $refree \leftarrow \{p_v : \{p_v\}\}_{p_v \in \mathcal{P}_v}$ 
29:          $refine \leftarrow True$ 
30:         break (both loops)
31: if  $refine$  then
32:    $p_{v,1}, p_{v,2}, rv', \mathcal{A}'_v, didrefine \leftarrow splitMode p_v^*, rv', \mathcal{A}'_v$ 
33:   if not  $didrefine$  then
34:     return:  $rv', \mathcal{A}'_v, \mathbf{O}'_v, Cache', refree, False, unsafe$ 
35:    $refree_{p_v} \leftarrow \{p_{v,1}, p_{v,2}\}$ 
36:    $Cache' p_{v,1} \leftarrow copy Cache' p_v^*$ 
37:    $Cache' p_{v,2} \leftarrow copy Cache' p_v^*$ 
38:   if  $parent = \perp$  then
39:     return:  $SymAR rv', \mathcal{A}'_v, rv' p_{init}, \perp, \emptyset, Cache', \mathbf{O}'_v$ 
40:   else
41:      $fixedpoint \leftarrow True$ 
42:     for  $p'_v \in refree_{p_v}^*$  do
43:        $\mathcal{A}'_v, \mathbf{O}'_v, Cache', curreftree, curfix, cursafe$ 
44:        $\leftarrow SymAR rv', \mathcal{A}'_v, p'_v, parent, R_v, Cache', \mathbf{O}'_v$ 
45:       if  $curfix = False$  then  $fixedpoint \leftarrow False$ 
46:        $refree \leftarrow refree \cup curreftree$ 
47:       if  $cursafe = unsafe$  then
48:         return:  $rv', \mathcal{A}'_v, \mathbf{O}'_v, Cache', refree, False, unsafe$ 
49: return:  $rv', \mathcal{A}'_v, \mathbf{O}'_v, Cache', refree, fixedpoint, safe$ 

```

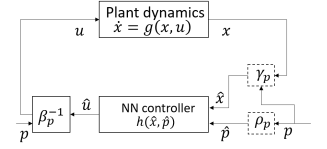
\mathcal{A} instead of \mathcal{A}_v , i.e. no abstraction used and no refinements, then SymAR will output safe for the call in equation (11).

5 SYMMETRY WITH NON-SYMMETRIC CONTROLLERS

We assumed so far that in the case of a control system, the controller h is symmetric. In some cases, h might not be symmetric. For example, the NN controller of the quadrotor in Section 2.2 is not symmetric with respect to rotations in the xy -plane. We show a counter example in Figure 2a.



(2a) NN controller of the quadrotor is not rotation symmetric.



(2b) Patching the controller to make it symmetric.

The NN input is the relative state $q - w$, which as we mentioned before, makes it symmetric to translations of the state and the reference trajectory. But, if we rotate the coordinate system of the physical xy -plane, i.e. rotate $p_x^q, p_y^q, v_x^q, v_y^q, b_x, b_y$ in equation (3), there is no guarantee that the NN will change its outputs θ and ϕ , such that the RHS of v_x^q , and $v_y^q, g \tan \theta$ and $-g \tan \phi$, are rotated accordingly.

Such non-symmetric controllers will prevent the dynamics from being equivariant. Equivariance is a desirable, and expected, property of certain dynamical systems. For example, vehicles dynamics are expected to be translation and rotation invariant in the xy -plane. Thus, non-symmetric controllers violate intuition about systems dynamics. Such controllers may not be feasible to abstract using Definition 4.2. Next, we will suggest a way to make any controller, including NN ones, such as that of the quadrotor, symmetric, leading to better controllers and retrieving the ability to construct abstractions.

Consider again the closed loop control system of equation (5). Let $\Phi = \{\gamma_p, \rho_p\}_{p \in \mathcal{P}}$ be a set of maps that we want it to be a virtual map of system (5). As before let us define $rv : \mathcal{P} \rightarrow \mathcal{P}$ by $rvp = \rho_p p$, for all $p \in \mathcal{P}$. Assume that for every $p \in \mathcal{P}$, there exists $\beta_p : \mathbf{U} \rightarrow \mathbf{U}$, such that the open loop dynamic function g is symmetric in the sense that it satisfies equation (6). Moreover, assume that $\gamma_{rvp}, \beta_{rvp}$, and ρ_{rvp} are identity maps for any $p \in \mathcal{P}$. This assumption means that applying the same symmetry transformation twice would not change the state nor the mode. Now, let us define a new controller $h' : \mathcal{X} \times \mathcal{P} \rightarrow \mathbf{U}$, that is shown in Figure 2b, as follows:

$$h'x, p = \beta_p^{-1} h \gamma_p x, rv p. \quad (12)$$

THEOREM 5.1. *For any $p \in \mathcal{P}$, the controller h' is β_p, γ_p, rv -symmetric.*

$$\begin{aligned}
& \text{PROOF. Fix } x \in \mathcal{X} \text{ and } p \in \mathcal{P}. \text{ Then, } \beta_p h' x, p \\
&= \beta_p \beta_p^{-1} h \gamma_p x, rvp, \text{ using equation (12),} \\
&= h \gamma_p x, rvp, \text{ since } \beta_p \beta_p^{-1} \text{ is the identity map,} \\
&= \beta_{rvp}^{-1} h \gamma_{rvp} \gamma_p x, \rho_{rvp} rvp, \\
& \quad [\text{since } \gamma_{rvp} \text{ and } \beta_{rvp} \text{ are identity maps, } \rho_{rvp} rvp = rvp], \\
&= h' \gamma_p x, rvp, \tag{13}
\end{aligned}$$

where the last equality follows from using equation (12) again. \square

The controller h' ensures that all modes $p \in \mathcal{P}$ that get mapped to the same mode p_v by rv have a transformed version, using β_p , of a unique control for the same transformed state $\gamma_p x$. That unique control is equal to h with mode p_v . This ensures that all modes that are equivalent under rv have symmetric behavior when the open loop dynamic function g is symmetric as well.

6 EXPERIMENTAL RESULTS

We implemented the symmetry abstraction refinement based safety verification method SymAR of Section 4.6 in Python3. We used DryVR [10] as a segment reachset computation tool in line 12 of SymAR.¹ We ran several experiments on different complex 2D and 3D scenarios having the quadrotor of Section 2.2 and a simple car with NN controllers to demonstrate the effectiveness of our approach in accelerating their safety verification.

6.1 Implementation details

The inputs to our implementation are scenarios and dynamics files defining the hybrid automaton \mathcal{A} along with the unsafe map \mathbf{O} . Its output is the boolean *issafe* indicating the safety verification result of the scenario, the refined abstract automaton \mathcal{A}_v , the corresponding unsafe map \mathbf{O}_v , and the reachset of \mathcal{A}_v .

The scenario file specifies: the initial set of states Θ_v , the planner output represented as a list of waypoints along with a list of edges defining the plan graph, a list of time horizons specifying the maximum time spent following any segment in the plan graph, and a list of boxes specifying the area around each waypoint at which it is considered reached, and a list of unsafe sets representing the obstacles in the environment that the agent is supposed to avoid. For quadrotor scenarios, we chose the time horizon for any edge to be $T = 5 \times \text{seg_length}$ and for the car, to be $T = \text{seg_length}$.

The dynamics file specifies the simulation function that simulates the agent forward from a specific initial state following a certain edge in the plan graph, the virtual map Φ as a list of three functions that implement γ_p , γ_p^{-1} , and rv . In case the controller is not symmetric as in the case of the quadrotor, β_p and β_p^{-1} are also provided to make the NN controller symmetric following Section 5.

Our implementation constructs an automaton \mathcal{A} , as in Section 2.2 for the plan graph that is produced by the planner. The set of modes \mathcal{P} considered is the set of segments of the plan, and the set of edges E represents the connected segments in the plan. The guards are constructed from the provided boxes around the waypoints and the resets are considered to be the identity function. It then uses the provided symmetry maps to construct the abstract automaton \mathcal{A}_v

along with the abstract unsafe map \mathbf{O}_v following Definition 4.2. If symmetry abstractions are being used, it then runs SymAR to compute the reachset of \mathcal{A}_v till a fixed point is reached or no more refinements are allowed and it is still unsafe. After that, it transforms the resulting reachset of \mathcal{A}_v to \mathcal{A} for plotting purposes. If symmetry is not being used, it proceeds into computing the reachset of \mathcal{A} directly and verifying its safety.

We use the RRT planner from [9] to construct plans from a single initial set to multiple destinations in 2D and 3D environments that are independent from the dynamics of the agents.

6.2 Scenarios and metrics

In addition to the quadrotor of Section 2.2 that we borrowed from [14], we trained a NN controller, a symmetric one, for a simple car with dynamics: $x = v * \cos \theta$; $y = v * \sin \theta$; $\dot{\theta} = \delta$. The details of the training and the controller are in the appendix.

We tested the car on three 2D complex plans in different environments with different obstacles, initial sets, goal sets, and paths. Those scenarios are in addition to the city like scenario in Figure 1. We tested the quadrotor on the same 2D environments as the car and three other 3D scenarios. All of the plans are in the appendix.

We experimented with two different virtual maps: (a) translation symmetry (SymT), where for any given mode, where a mode is a segment in the plan, the symmetry maps the states and the segment to the coordinate system centered at the end waypoint of the segment, and (b) rotation and translation symmetry (SymTR), where instead of just translation of the origin of the coordinate system, we rotate the xy -plane so that the segment is aligned with the y -axis.

Finally, and most importantly, we experiment with different refinement thresholds, where we allow SymAR to refine only a limited number of times to check the benefits of having refinement when using symmetry based abstractions for safety verification, especially when the automaton under consideration has complex dynamics because of a NN controller.

Next section, we compare different experiments according to the following statistics: time (min), being the total verification time, # rd, is the number of refinements done, # rt, is the number of refinements threshold, $|\mathcal{P}|$, $|E|$, $|\mathcal{P}_v|$, $|E_v|$, # co, is the number of calls to the reachtube computation engine DryVR, # tr, is the number of reachsets that had to be transformed from \mathcal{A}_v to construct the reachset \mathcal{A} , and *issafe*, to indicate the safety verification result.

The different colors used in the figures correspond to the reachsets of different abstract modes. That is the reason why in the NoS case, the whole reachset has the same color, while the number of colors increase with number of refinements as in Figures 1 and 3. The corresponding abstract reachsets for both figures are in the appendix.

6.3 Results and analysis

To have a comprehensive look at our experimental results, please check tables 5 and 6 in the appendix. Here, we select few results to highlight few observations regarding the benefits of refinement and the choice of virtual map used to construct \mathcal{A}_v .

Choice of refine thresholds. To show the effect of refinements on the ability for the usage of abstractions to accelerate safety verification, we show the results of running our implementation on two scenarios using SymTR and different refine thresholds in Table 1.

¹We experimented as well using Verisig [14], but it has been significantly slower than DryVR. The latter spent around 20 hours in the computation of the reachsets of five modes of the quadrotor, which left us with the DryVR option because of time constraints.

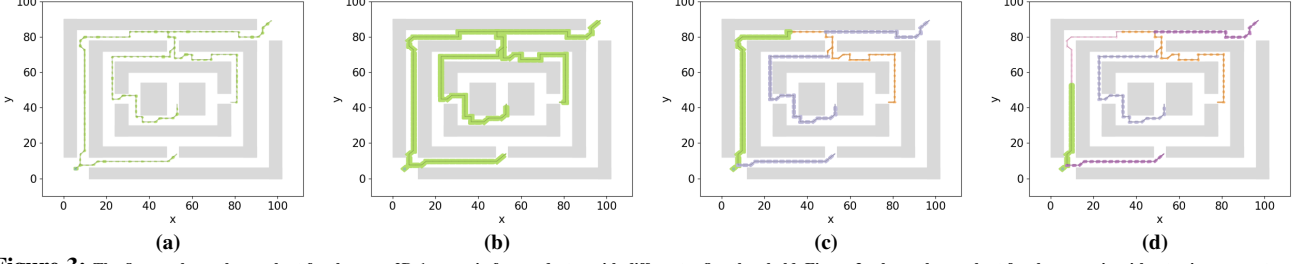


Figure 3: The figures shows the reachset for the comp2D-1 scenario for quadrotor with different refine threshold. Figure 3a shows the reachset for the scenario without using symmetry and we can see clearly that the result is safe. Figure 3b shows the reachset for the scenario without using refinement. We can see that the reachset overbloats. Figure 3c shows the reachset for the scenario with refine threshold 10. The reachset is more conservative compared with not using refinement, but the result is still different from that from not using symmetry. Figure 3d shows the reachset for the scenario with refine threshold 50 and the actual number of refinement is 3. With enough refinement, the verification result is safe, which is the same as not using symmetry.

In the NoS case, the verification result is safe for both scenarios and the computed reachset for comp2D-1 scenario is plotted in figure 3a. In the SymTR case, but without refinement (refine threshold 0), we can see that the amount of time for verification is 96.0% faster than the NoS case for scenario comp2D-1 and 98.6% faster than the NoS case for scenario comp2D-2. However, the verification result is not safe for both scenarios. The computed reachset for scenario comp2D-1 is plotted in Figure 3b, where it is clear that the reachset is intersecting the obstacles.

With refine threshold 2, for both scenarios, the running time is longer than with refine threshold 0 and the verification is still unsafe, which does not match what we get in the NoS case. The obtained reachset for scenario comp2D-1 is plotted in Figure 3c. We can see from the plot that the computed reachset is tighter than that corresponding to refine threshold 0, but not enough to prove safety.

When refine threshold 10 is used, the verification result is safe, matching the NoS case. The number of refinement for scenario comp2D-1 is 3 and the number of refinement for scenario comp2D-2 is 5. However, even with refinement, the amount of time it takes for verifying both scenarios is still significantly faster than the NoS case. For the comp2D-1 scenario, with SymTR, the amount of time required for verification is 83.8% faster than the NoS case and for scenario com2D-2, it is 89.8% faster. The reachset for scenario comp2D-1 with refine threshold 10 is shown in Figure 3d. We can see from the figure that the computed reachset is tighter than both those corresponding to using refine threshold 2 and without refinement.

Table 1: Comparison between different refine thresholds.

Agent	quadrotor-comp2D-1				quadrotor-comp2D-2			
stats	SymTR			NoS	SymTR			NoS
time	1.47	9.21	6.01	37.12	3.49	26.83	25.29	248.16
$ \mathcal{P} $	140	140	140	48	458	458	458	264
$ E $	139	139	139	47	457	457	457	263
# co	1	12	10	96	1	11	16	264
issafe	False	False	True	True	False	False	True	True
# rt	0	2	10	NA	0	2	10	NA
# rd	0	2	3	NA	0	2	5	NA
$ \mathcal{P}_v $	1	3	5	NA	1	3	6	NA
$ E_v $	19	6	12	NA	1	6	16	NA
# tr	140	420	175	NA	458	1145	831	NA

NoS vs SymT vs SymTR. The result of running our implementation on two different scenarios with NoS, SymT, SymTR is shown in Table 2. For the presented results, we can see that with symmetry, our implementation is significantly faster than the NoS case. With SymT, for the comp2D-1 scenario, the running time reduced by 87.9%

and for comp2D-2 scenario, the running time reduced by 39.0%. With SymTR, for the comp2D-1 scenario, the running time reduced by 83.8% and for comp2D-2 scenario, the running time reduced by 89.8%. In addition, we can see that the number of calls to the reachset computer while using symmetry decreased comparing with not using symmetry. When comparing between using SymT and SymTR, we observed that for comp2D-1 scenario, using SymTR is slower then using SymT. Since with both translation and rotation symmetry, the computed reachset can be more conservative and therefore, may require a higher number of refinements as the example illustrates. Thus, for the comp2D-1 scenario, our tool has to make more calls to DryVR while using SymTR compared with using SymT.

However, for the comp2D-2 scenario, using SymTR is actually faster then using SymT. Although, using SymT still requires less number of refinement compared with using SymTR, Less number of tubes are actually computed and transformed. Therefore, causing the tool to run faster with SymTR.

Table 2: NoS vs SymT vs SymTR.

Agent Quadrotor	SymTR		SymT		NoS	
stats \ comp2D-	1	2	1	2	1	2
time	6.01	25.29	4.50	151.26	19.25	248.16
$ \mathcal{P} $	140	458	140	458	48	264
$ E $	139	457	139	457	47	263
# co	10	16	8	27	48	264
issafe	True	True	True	True	True	True
# rt	10	10	10	10	NA	NA
# rd	3	5	0	3	NA	NA
$ \mathcal{P}_v $	5	6	7	10	NA	NA
$ E_v $	175	831	344	3825	NA	NA

7 CONCLUSIONS

We presented an algorithm to refine symmetry-based abstractions in the context of safety verification. We showed how to the algorithm selects abstract modes to split based on their role in causing a safety violation. Moreover, we extended this type of abstractions to closed-loop control systems, showing the properties that the controller should satisfy for the abstraction to be feasible. We further showed how to append non-symmetric controllers such as NN with symmetry transformations of their inputs and outputs so that symmetry-abstractions would be possible. Finally, we showed significant savings in safety verification times of NN-controlled quadrotor and car following complex paths in 2D and 3D environments.

REFERENCES

- [1] M. Althoff. 2015. An Introduction to CORA 2015. In *Proc. of the Workshop on Applied Verification for Continuous and Hybrid Systems*.
- [2] R. Alur, C. Courcoubetis, T. A. Henzinger, and P. H. Ho. 1993. Hybrid automata: an algorithmic approach to the specification and verification of hybrid systems. In *Hybrid Systems (LNCS, Vol. 736)*, R. L. Grossman, A. Nerode, A. P. Ravn, and H. Rischel (Eds.), Springer-Verlag, 209–229.
- [3] Stanley Bak and Parasara Sridhar Duggirala. 2017. Hylaa: A tool for computing simulation-equivalent reachability for linear systems. In *Proceedings of the 20th International Conference on Hybrid Systems: Computation and Control*. ACM, 173–178.
- [4] Xin Chen, Erika Ábrahám, and Sriram Sankaranarayanan. 2013. Flow*: An analyzer for non-linear hybrid systems. In *CAV*. Springer, 258–263.
- [5] Xin Chen, Sriram Sankaranarayanan, and Erika Abraham. 2015. Flow* 1.2: More Effective to Play with Hybrid Systems. In *ARCH14-15. 1st and 2nd International Workshop on Applied Verification for Continuous and Hybrid Systems (EPIC Series in Computing, Vol. 34)*, Goran Frehse and Matthias Althoff (Eds.), EasyChair, 152–159. <https://doi.org/10.29007/1w4t>
- [6] Parasara Sridhar Duggirala, Chuchu Fan, Sayan Mitra, and Mahesh Viswanathan. 2015. Meeting a Powertrain Verification Challenge. In *Computer Aided Verification - 27th International Conference, CAV 2015, San Francisco, CA, USA, July 18-24, 2015, Proceedings, Part I*. 536–543. https://doi.org/10.1007/978-3-319-21690-4_37
- [7] Parasara Sridhar Duggirala, Sayan Mitra, Mahesh Viswanathan, and Matthew Potok. 2015. C2E2: A Verification Tool for Stateflow Models. In *Proceedings of the 21st International Conference on Tools and Algorithms for the Construction and Analysis of Systems - Volume 9035*. Springer-Verlag, Berlin, Heidelberg, 68–82. https://doi.org/10.1007/978-3-662-46681-0_5
- [8] Souradeep Dutta, Xin Chen, Susmit Jha, Sriram Sankaranarayanan, and Ashish Tiwari. 2019. Sherlock - A Tool for Verification of Neural Network Feedback Systems: Demo Abstract. In *Proceedings of the 22nd ACM International Conference on Hybrid Systems: Computation and Control (Montreal, Quebec, Canada) (HSCC '19)*. Association for Computing Machinery, New York, NY, USA, 262–263. <https://doi.org/10.1145/3302504.3313351>
- [9] Chuchu Fan, Kristina Miller, and Sayan Mitra. 2020. Fast and Guaranteed Safe Controller Synthesis for Nonlinear Vehicle Models. In *Computer Aided Verification, Shuvendu K. Lahiri and Chao Wang (Eds.)*. Springer International Publishing, Cham, 629–652.
- [10] Chuchu Fan, Bolun Qi, Sayan Mitra, and Mahesh Viswanathan. 2017. DryVR: Data-Driven Verification and Compositional Reasoning for Automotive Systems. In *Computer Aided Verification, Rupak Majumdar and Viktor Kunčák (Eds.)*. Springer International Publishing, Cham, 441–461.
- [11] Chuchu Fan, Bolun Qi, Sayan Mitra, Mahesh Viswanathan, and Parasara Sridhar Duggirala. 2016. Automatic Reachability Analysis for Nonlinear Hybrid Models with C2E2. In *Computer Aided Verification - 28th International Conference, CAV 2016, Toronto, ON, Canada, July 17-23, 2016, Proceedings, Part I*. 531–538. https://doi.org/10.1007/978-3-319-41528-4_29
- [12] Goran Frehse, Colas Le Guernic, Alexandre Donzé, Scott Cotton, Rajarshi Ray, Olivier Lebeltel, Rodolfo Ripado, Antoine Girard, Thao Dang, and Oded Maler. 2011. SpaceEx: Scalable Verification of Hybrid Systems. In *CAV*. 379–395.
- [13] Thomas A. Henzinger. 1996. The Theory of Hybrid Automata. In *11th Annual IEEE Symposium on Logic in Computer Science*. 278–292.
- [14] Radoslav Ivanov, James Weimer, Rajeev Alur, George J Pappas, and Insup Lee. 2019. Verisig: verifying safety properties of hybrid systems with neural network controllers. In *Proceedings of the 22nd ACM International Conference on Hybrid Systems: Computation and Control*. 169–178.
- [15] Dilsun K. Kaynar, Nancy Lynch, Roberto Segala, and Frits Vaandrager. 2005. *The Theory of Timed I/O Automata*. Morgan Claypool. Also available as Technical Report MIT-LCS-TR-917, MIT.
- [16] Steven M. Lavalley. 1998. *Rapidly-Exploring Random Trees: A New Tool for Path Planning*. Technical Report.
- [17] Sayan Mitra. 2007. *A Verification Framework for Hybrid Systems*. Ph.D. Dissertation. Massachusetts Institute of Technology, Cambridge, MA 02139. <http://people.csail.mit.edu/mitras/research/thesis.pdf>
- [18] Nima Roohi, Yu Wang, Matthew West, Geir Dullerud, and Mahesh Viswanathan. 2017. Statistical Verification of Toyota Powertrain Control Verification Benchmark. In *Proceedings of the 20th international conference on Hybrid systems: computation and control*. ACM.
- [19] Giovanni Russo and Jean-Jacques E Slotine. 2011. Symmetries, stability, and control in nonlinear systems and networks. *Physical Review E* 84, 4 (2011), 041929.
- [20] Hussein Sibai and Sayan Mitra. 2020. Symmetry Abstractions for Hybrid Systems and their Applications. *arXiv:2006.09485 [eess.SY]*
- [21] Hoang-Dung Tran, Xiaodong Yang, Diego Manzananas Lopez, Patrick Musau, Luan Viet Nguyen, Weiming Xiang, Stanley Bak, and Taylor T. Johnson. 2020. NNV: The Neural Network Verification Tool for Deep Neural Networks and

Learning-Enabled Cyber-Physical Systems. In *Computer Aided Verification*, Shuvendu K. Lahiri and Chao Wang (Eds.). Springer International Publishing, Cham, 3–17.

A ADDITIONAL EXPERIMENTAL RESULTS

A.1 Car NN controller

The controller is trained to drive the car to follow a straight reference trajectory aligned with positive y-direction towards the origin. The controller follows method explained in Section 5 and any given reference segment to be aligned with the y-axis and compute corresponding control inputs.

The inputs to the controller are the relative position of the car in the plane with respect to the reference position in the segment being followed and the cosine and sine of the relative orientation of the car with respect to the orientation of the segment being followed. The outputs from the controller are the speed v of the vehicle and the steering angle δ of the vehicle. The neural network have 1 hidden layer with 100 hidden neurons.

The training data for this controller is obtained by random sampling positions in range $x \in [-3, 3]$ and $y \in [-2.5, 1.5]$ and orientation in range $\theta \in [0, \pi]$. During the training process, the vehicle will start from the sampled position and orientation and drive towards the origin $[x, y, \theta] = [0, 0, \frac{\pi}{2}]$ which is the reference state.

A.2 Long segments vs Short segments without using symmetry

To further utilize the symmetry property of the scenario, we will split mode that contains longer segments into several modes that contains shorter segments with equal length. In table 3 shows the statistics for verifying the comp2D-1 scenario for quadrotor without using symmetry. For experiment run comp2D-1-S, modes that contain segments with length larger than 3 is split into mode that contain segments with length smaller than or equal to 3. For experiment run comp2D-1, the modes are not split. The experiment is to compare the effect of splitting longer segments into short segments while not using symmetry. From the collected data, we can see that although number of modes and number calls to reachset computer increase, the amount of time it takes for verification of the scenarios is not influenced. Therefore, for the rest of the experiments, while not using symmetry, we are verifying scenarios without splitting modes.

Table 3: Results showing that without using symmetry, splitting modes with longer segments to modes with shorter ones won't influence performance.

Experiment run	complex2D-1	complex2D-1-S
# original modes	48	140
# virtual modes	47	139
# computed tubes	96	280
# segs computed	48	140
time	37.12	36.45

A.3 Effect of model dynamics

The stats in table 4 compare the influence of agent dynamics have on the performance of verification. In this experiment, we are trying

to verify the comp2D-1 scenario with different agents and compare the performance. For both agents, we will run verification with both no symmetry and symmetry with translation and rotation. While running with SymTR, we will also try different refinement thresholds.

Table 4: Comparison between different agent dynamics.

	car-comp2D-1				quadrotor-comp2D-1			
stats	SymTR			NoS	SymTR			NoS
time	4.58	21.23	39.5	44.66	1.47	9.21	6.01	37.12
$ \mathcal{P} $	140	140	140	48	140	140	140	48
$ E $	139	139	139	47	139	139	139	47
# co	6	84	135	96	1	12	10	96
issafe	F	F	T	T	F	F	T	T
# rt	0	10	50	NA	0	2	10	NA
# rd	0	10	17	NA	0	2	3	NA
$ \mathcal{P}_v $	1	11	18	NA	1	3	5	NA
$ E_v $	1	29	47	NA	19	6	12	NA
# tr	840	761	1132	NA	140	420	175	NA

From the statistics, we can see that without symmetry, the amount of time required for verify the scenario with car or quadrotor is relatively close. However, with both translation and rotation symmetry, since the quadrotor have more stable controller and more symmetric dynamics, the number of refinements required for verifying the quadrotor scenario is much less then the number of refinements required for verifying the car scenario. In addition, since the dynamics of quadrotor is more symmetric than the car, it is able to reach the fixed point earlier than the car. Therefore, it takes much less time to verify the scenario with quadrotor than verify the scenario with the car.

Table 5: Results for quadrotor.

tool \ agent model		Quadrotor												
tool	stats	comp2D-1			comp2D-2			comp2D-3			comp3D-1			comp3D-2
SymTR	# rt	0	2	10	0	2	10	0	2	10	0	1	10	0
	# rd	0	2	3	0	2	5	0	2	4	0	1	2	0
	time	1.47	9.21	6.01	3.49	26.83	25.29	8.16	19.47	25.114	11.66	38.30	41.34	24.75
	$ \mathcal{P} $	140	140	140	458	458	458	520	520	520	96	96	96	188
	$ E $	139	139	139	457	457	457	519	519	519	95	95	95	187
	$ \mathcal{P}_v $	1	3	5	1	3	6	1	3	5	4	5	6	3
	$ E_v $	19	6	12	1	6	16	1	6	13	9	17	24	7
	# co	1	12	10	1	11	16	2	12	20	16	25	37	18
	# tr	140	420	175	458	1145	831	1040	1430	1430	400	972	1016	868
	# segs computed	1	5	9	1	5	11	1	-5	9	4	8	12	3
	# segs transformed	140	140	140	458	458	458	520	520	520	96	96	96	188
	# tubes per segs	1.0	2.4	1.11	1.0	2.2	1.45	2.0	2.4	2.22	4.0	5.75	5.08	6.0
	issafe	False	False	True	False	False	True	False	False	True	False	False	True	True
SymT	# rt	0	2	10	0	2	10	0	2	10	0	1	10	0
	# rd	0	0	0	0	2	3	0	0	2	0	0	0	0
	time	7.19	7.49	4.50	34.96	86.76	151.26	23.43	24.02	59.01	117.51	117.94	116.74	99.17
	$ \mathcal{P} $	140	140	140	458	458	458	520	520	520	96	96	96	188
	$ E $	139	139	139	457	457	457	519	519	519	95	95	95	187
	$ \mathcal{P}_v $	7	7	7	7	9	10	7	7	9	11	11	11	10
	$ E_v $	19	19	19	30	46	53	30	30	48	42	42	42	57
	# co	9	15	8	15	33	27	20	20	34	32	32	32	35
	# tr	385	572	344	1151	2220	3825	1842	1842	3480	3284	3284	3284	2470
	# segs computed	12	9	9	10	16	29	10	10	16	24	24	24	20
	# segs transformed	140	140	140	458	458	458	520	520	520	96	86	96	188
	# tubes per segs	1.17	2.22	1.22	2.3	3.25	5.38	2.9	2.9	3.81	7.42	7.42	7.42	5.9
	issafe	True	True	True	False	False	True	False	True	True	True	True	True	True
NoS	time	37.12			248.16			288.54			34.32			99.92
	$ \mathcal{P} $	48			264			105			56			122
	$ E $	47			263			104			55			121
	$ \mathcal{P}_v $	96			264			210			112			244
	$ E_v $	48			264			105			56			122
	# tubes per segs	2.0			1.0			2.0			2.0			2.0
	issafe	True			True			True			True			True

Table 6: Results for car.

tool \ agent model		Car				
tool	stats	comp2D-1			comp2D-3	
SymTR-DryVR	# rt	0	10	50	0	50
	# rd	0	10	17	0	10
	time	4.58	21.23	39.5	26.54	192.32
	$ \mathcal{P} $	140	140	140	520	520
	$ E $	139	139	139	519	519
	$ \mathcal{P}_v $	1	11	18	1	11
	$ E_v $	1	29	47	1	33
	# co	6	84	135	11	125
	# tr	840	761	1132	5720	17506
	# segs computed	2	30	41	4	43
	# segs transformed	140	140	140	520	520
	# tubes per segs	3.0	2.8	3.59	2.75	6.02
issafe	False	False	True	False	True	
SymT-DryVR	# rt	0	10	50	NA	NA
	# rd	0	6	0	NA	NA
	time	23.80	26.02	22.43	NA	NA
	$ \mathcal{P} $	140	140	140	NA	NA
	$ E $	139	139	139	NA	NA
	$ \mathcal{P}_v $	7	13	7	NA	NA
	$ E_v $	19	52	19	NA	NA
	# co	29	84	25	NA	NA
	# tr	1520	934	1364	NA	NA
	# segs computed	14	35	14	NA	NA
	# segs transformed	140	140	140	NA	NA
	# tubes per segs	3.36	26.02	2.93	NA	NA
	issafe	True	True	True	NA	NA
NoSym-DryVR	time	44.66			195.71	
	$ \mathcal{P} $	48			105	
	$ E $	47			104	
	# co	96			210	
	# tr	0			0	
	# segs computed	48			105	
	# segs transformed	0			0	
	# tubes per segs	2.0			2.0	
	issafe	True			True	

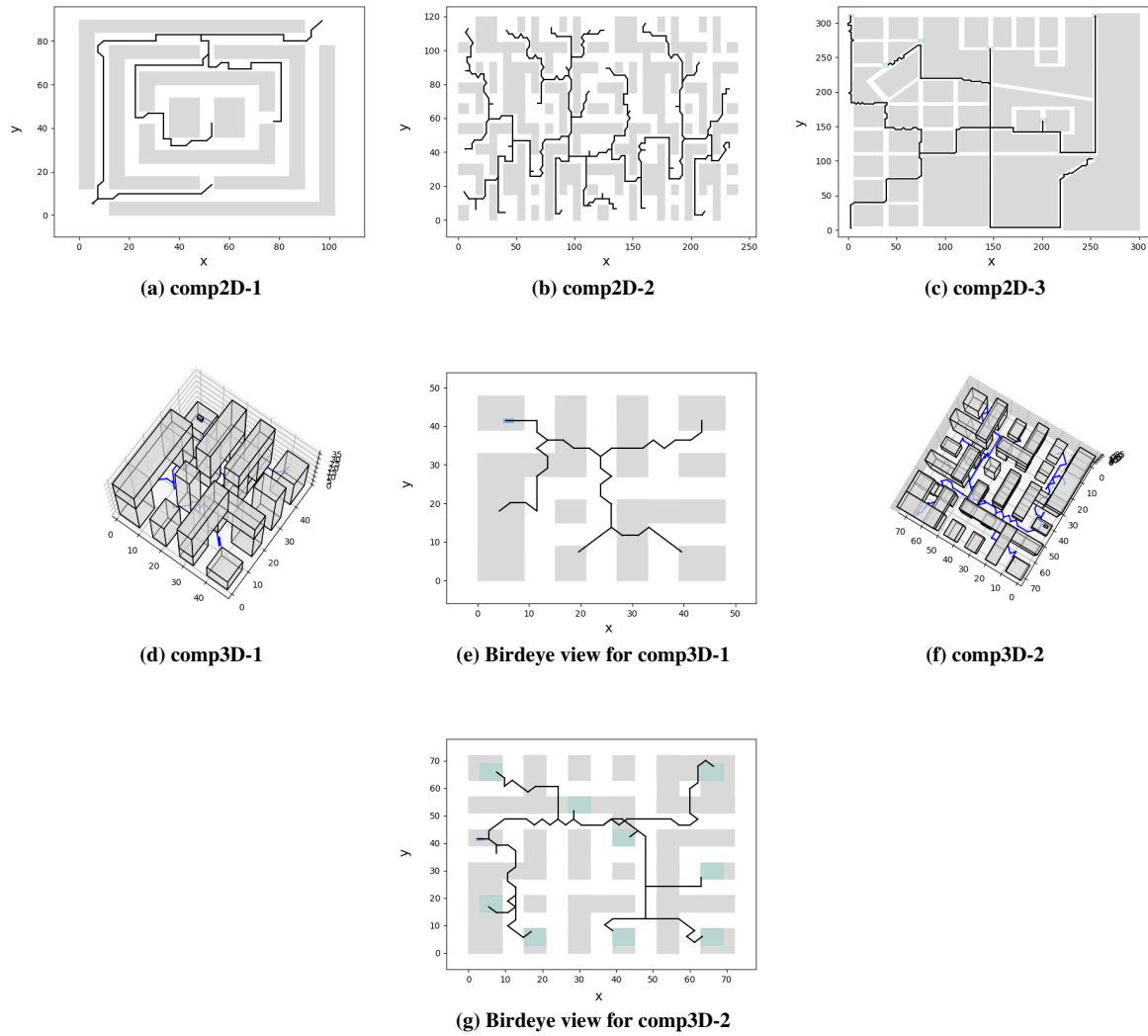


Figure 4: The figures shows the scenarios and planned path that we run the experiment with.

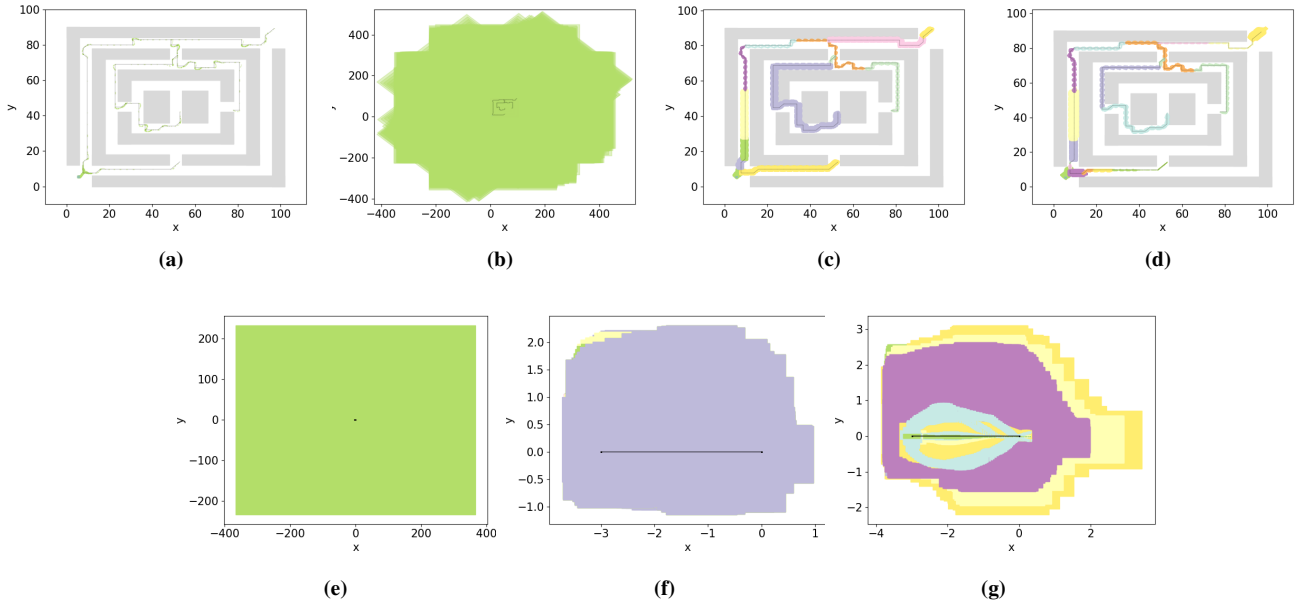


Figure 5: The figures shows the reachset for the comp2D-1 scenario for car with different refine threshold. Figure 5a shows the reachset for the scenario without using symmetry and we can see clearly that the result is safe. Figure 5b shows the original reachset for the scenario without using refinement. We can see that the reachset overbloats. The virtual reachsets for the scenario are plotter in figure 5e. Figure 5c shows the original reachset for the scenario with refine threshold 10. The reachset is more conservative compared with not using refinement, but the result is still different from that from not using symmetry. The virtual reachsets for the scenario are plotter in figure 5f. Figure 5d shows the original reachset for the scenario with refine threshold 50 and the actual number of refinement is 17. With enough refinement, the verification result is safe, which is the same as not using symmetry. The virtual reachsets for the scenario are plotter in figure 5g.

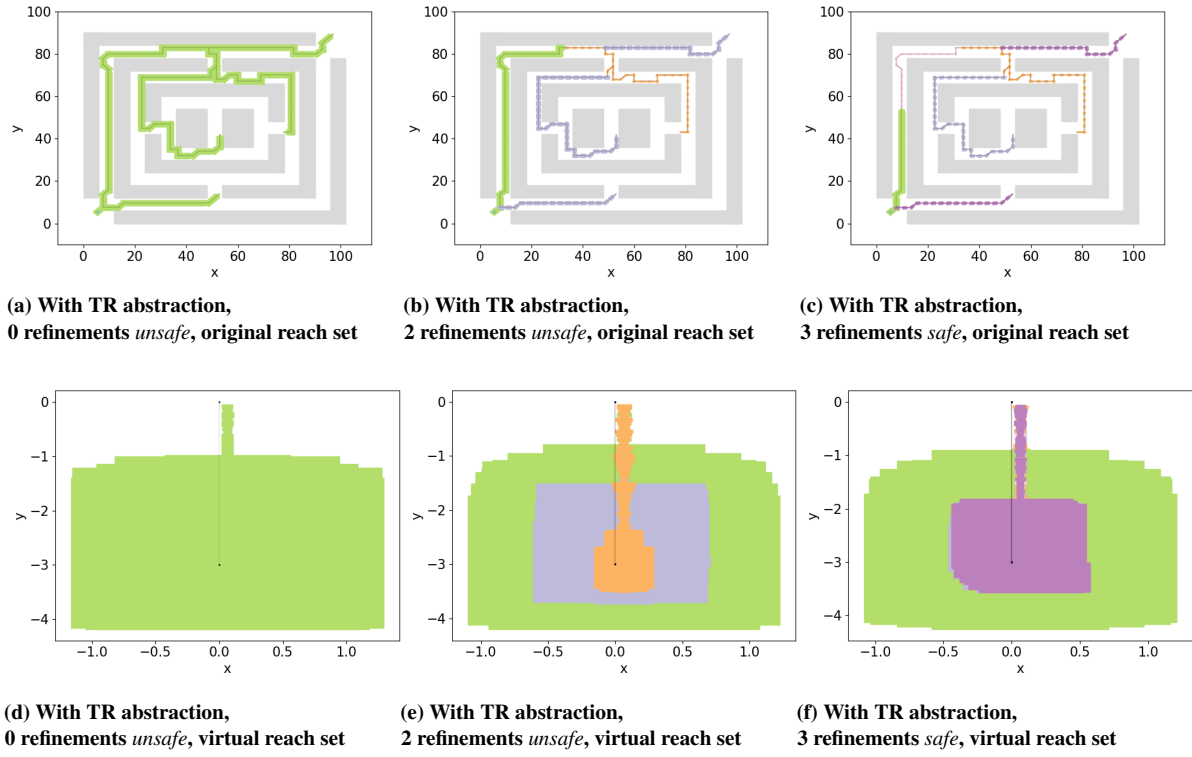


Figure 6: Safety verification of a NN-controlled quadrotor in scenario comp2D-1 using SymAR.

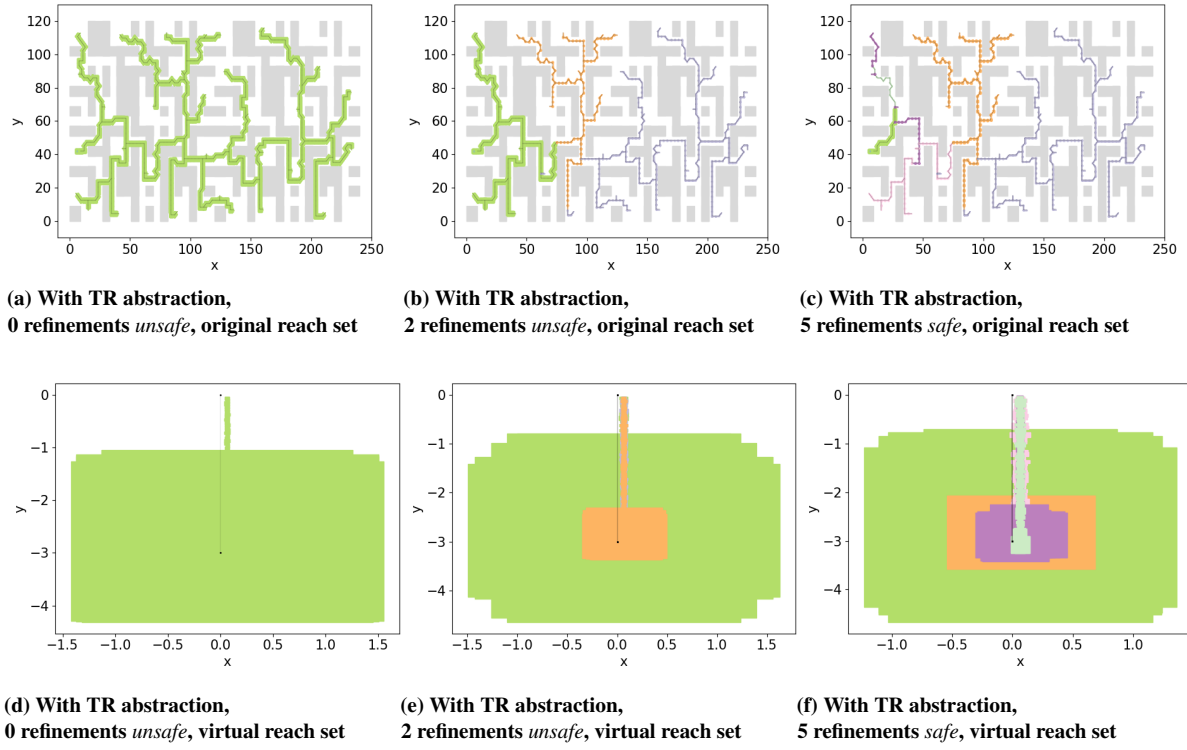


Figure 7: Safety verification of a NN-controlled quadrotor in scenario comp2D-2 using SymAR.

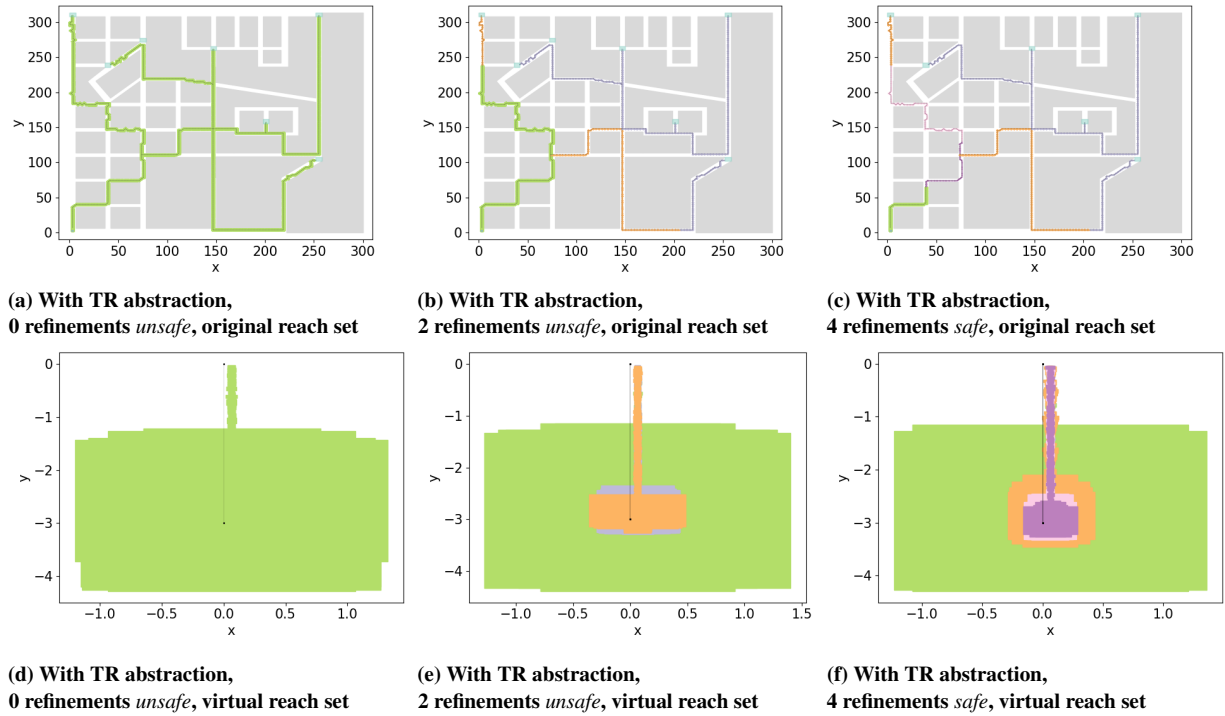


Figure 8: Safety verification of a NN-controlled quadrotor in scenario comp2D-3 using SymAR.

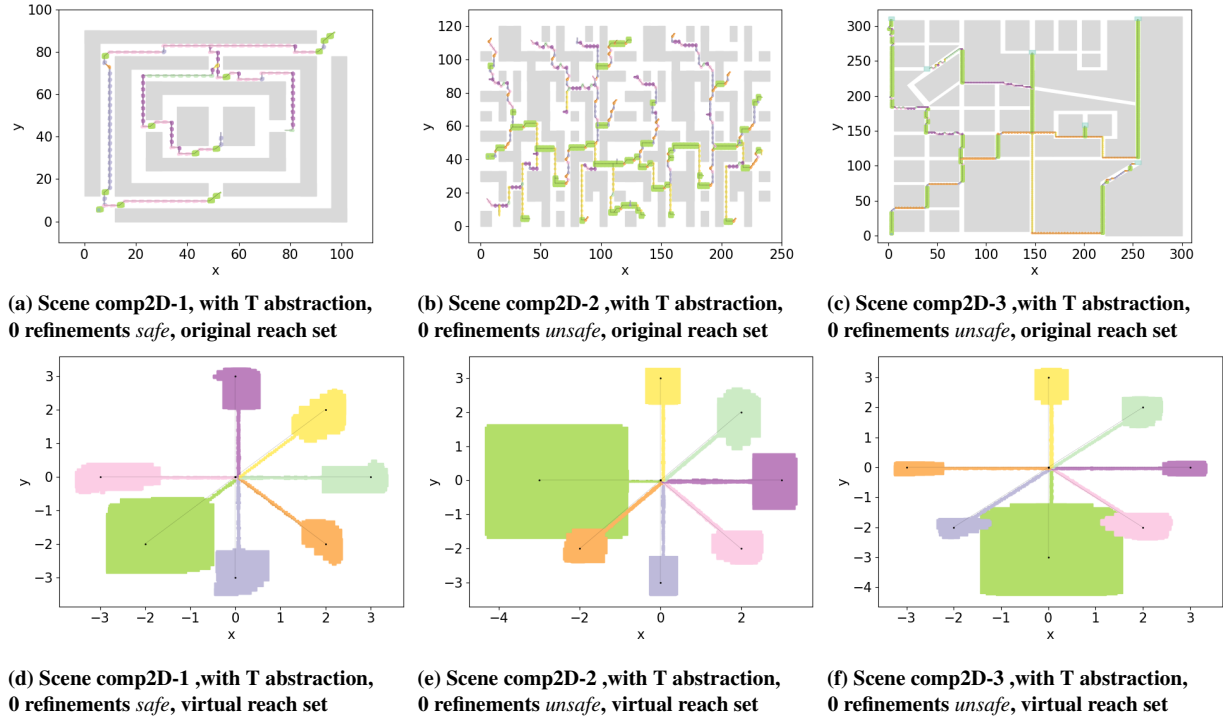


Figure 9: Safety verification of a NN-controlled quadrotor in scenario comp2D-3 using SymAR.